3D numerical study of the effect of aspect ratios on mixed convection air flow in upward solar air heater

A. Boulemtafes-Boukadoum, Cherifa Abid, A. Benzaoui

3D numerical study of the effect of aspect ratios on mixed convection air flow in upward solar air heater

A.Boulemtafes-Boukadoum[1*], C.Abid[2], A. Benzaoui[3]

[1]Centre de Developpement des Energies Renouvelables, CDER, 16340, Algiers, Algeria
*corresponding author a.boulemtafes@cder.dz, aboukadoum@gmail.com
[2]Aix Marseille Univ, CNRS, IUSTI, Marseille, France
cherifa.abid@univ-amu.fr
[3] Laboratoire de Thermodynamique et des Systèmes Énergétiques, USTHB, 16111Algiers, Algeria
abenzaoui@gmail.com

Abstract
3D Numerical study of mixed convection air flow in upward solar air heater with large spanwise aspect ratio (A = 10 to 40) was performed using CFD commercial code Fluent14.5 (ANSYS).The main objective of this study is to investigate the channel height's effect (Aspect ratio) on flow pattern and heat transfer in upward solar air heater in the particular case of low Re and high aspect ratio. The bottom plate (absorber) was submitted to Constant Heat Flux (CHF) in the range of 200 to 1000 W/m2 and Reynolds number was varied from 50 to 1000. The simulation results of flow visualization and Nusselt number calculation show that depending on Ri*, the velocity and temperature distribution in SAH vary greatly with channel's height. Our results are in concordance with most of authors conclusions about Poiseuille-Rayleigh-Benard flows. In mixed convection, increasing heat flux enhance heat transfer unlike forced convection flows. Simulation results of flow visualization and Nusselt number calculation have shown that depending on Ri*, the velocity and temperature distribution in SAH vary greatly with the channel's height. The obtained results were different from previous studies. Indeed, our investigation of channel's height was achieved for the same heat flux but different Grashof number. For low channel's height (high aspect ratio), enhancing heat flux has not a significant effect but for higher channel's height, an augmentation of heat flux enhance buoyancy effects in the flow and causes high turbulence, Also, increasing Reynolds number in low channel's height (high A), can enhance substantially heat transfer . For higher channel's height (low A), increasing Reynolds number decrease Ri* and thus buoyancy forces. Heat transfer is reduced and so Nusselt number. Those results may be very useful for engineers in designing and testing solar collectors.
Keywords: Unsteady, mixed convection, CFD, solar collector, PRB flow, heat transfer, duct height.

1. Introduction

Mixed convection is a heat transfer mode where free convection phenomena coexist along those of forced convection ones. When buoyancy is small compared to inertia, mixed convective flow is simple and steady. But when the buoyancy is dominated over the inertia, the flow can become unsteady, transitional and even turbulent. Additionally, various complex flow structures like longitudinal vortices, transverse waves and flow reversal may appear during this buoyancy induced flow transition (Lin and Lin 1996b).
Mixed convective heat transfer is a complex mechanism and understanding this process helps to improve design and optimization of energy devices by reducing heat losses and enhancing efficiency. Mixed convection is prevailing in wide range of engineering

applications (Wessels et al. 2019). Detailed understanding of these buoyancy induced flow is important in fundamental fluid mechanics and heat transfer studies such as cooling of microelectronic components, heat transfer in compact heat exchangers, growth of single crystal through chemical vapor deposition (Lin and Lin 1996b), chemical and nuclear power, and in renewable energies as solar collectors (Abid et al. 2006). Mixed convection studies are

Nomenclature

C_p	constant-pressure specific heat of air
D	hydraulique diameter
e	glass thickness
g	gravitational acceleration
G	incident solar radiation intensity on the solar air heater
H	channel's height
h	local convective heat transfer coefficient
h_w	heat transfer coefficient between glazing and the external surrounding air
k	air thermal conductivity
L	channel's length
$\dot{m}$	air mass flow rate
P	pressure
Q	heat flux imposed on the absorber
q	useful energy gain
S	aperture area of SAH
T	temperature
U	air averaged velocity in the duct
u	longitudinal velocity component
v	transversal velocity component
w	azimuthal velocity component
W	channel's width

Dimensionless numbers/parameters

$Gr^* = \frac{g\beta Q H^4}{k\nu^2}$	modified Grashoff number
$Nu(x) = \frac{h(x)H}{k}$	local Nusselt number
$Re = \frac{UH}{\nu}$	Reynolds number
$Ri^*=Gr^*/Re^2$	modified Richardson number
A=W/H	Channel's spanwise Aspect ratio
$X^+=X/L$	Dimensionless abscissa
1/Gz=x/RePrD	Inverse Graetz number

Greek letters

ε	glazing emissivity
θ	inclination angle
σ	stefan-boltzmann coefficient
β	air thermal expansion coefficient
ν	air kinematic viscosity

Subscripts

abs, p	absorber, bottom wall
amb	ambient

atm	atmospheric
b	bulk
g	glazing, top wall
i	inlet
o	outlet
s	sky

still relevant, many recent scientific papers are related to this heat transfer mode over the world. (Wessels et al. 2019; Chakkingal et al. 2020; Taher and Abid 2018; Zhu et al. 2020).

Mixed convection heat transfer mode has been investigated both experimentally and numerically in a wide range of scientific papers. Most of those studies were about mixed convection between parallel plates or in rectangular channel heated from below, called Poiseuille-Rayleigh-Benard flows (PRB). In PRB flows at relatively low Reynolds and Rayleigh numbers, the combination of Rayleigh-Bénard cells with a Poiseuille flow give rise to very complex flow structures ranging from time-dependant transverse rolls to steady longitudinal rolls time-dependent mixed rolls and time- oscillating rolls (wavy, snaking or varicose) (Benzaoui, Nicolas, and Xin 2005). An exhaustive bibliographical review on the PRB flows was achieved by (Nicolas 2002). The study of Mori and Uchida (Uchida 1966) is considered as one of the first experimental studies on mixed convection of air flow between two horizontal parallel plates, where they could observe longitudinal rolls. According to literature, the longitudinal rolls appear as soon as Ra exceeds the critical value of 1708. (Ostrach and Kamotani 1975) have shown experimentally that these rolls become unstable as soon as Ra> 8000. Other authors have noticed that the rolls structure is destroyed beyond Ra = 18000. (Abid et al. 2006) observed an original structure composed of two longitudinal rolls nested in a large transverse roll in the case of water laminar flow in a rectangular pipe (A=2) during stationary regime. Based on numerical and experimental study, (Benderradji et al. 2008) have noted for the first time the existence of two mechanisms of roll initiation in a horizontal channel uniformly heated from below at constant heat flux for water flow. The first initiation mechanism is due to lateral wall effect and the second one combines the wall effect with the existence of high vertical temperature gradient in the boundary layer at the bottom of the channel, which simultaneously triggers pairs of rolls in the whole zone between the two lateral rolls (Benderradji et al. 2008).

Most of those studies revealed that buoyancy forces have a great effect on increasing heat transfer in mixed convection flows. In the entry region, (Kamotani, Ostrach, and Miao 1979) noted that heat transfer depends not only on Rayleigh number but also on $Ri=Gr/Re^2$ which expresses the ratio of buoyancy forces to inertia forces. (Lin and Lin 1996a) explored experimentally the effect of Reynolds and Grashof numbers on the transition of mixed convection flow in a bottom-heated pipe. One of the main results obtained is that the buoyancy forces tend to thicken the boundary layer in the inlet region of the channel before the onset of instability. The Nusselt number tends to fall below the asymptotic value of the case of forced convection, but heat transfer is increased after the onset of instability. (Maughan and Incropera 1990) studied numerically the increase in heat transfer for air flow between two parallel plates heated from below. Their results showed that for large values of heat flux and flow rate, there is a sensitive enhancement of heat transfer prior to the establishment of thermal instability. Experimental measurements and visualization confirmed this result.

(Gau et al. 1999) highlighted the effect of Ri on Nusselt number and they observed that when Ri increases, the locations for both heat transfer enhancement onset and maximum Nusselt number move upstream. In the literature and for heat transfer, some stability analysis express the Nusselt number as a function of Reynolds (*Re*), Rayleigh (*Ra*), and Prandtl (*Pr*) numbers and also of the transverse aspect ratio A (width to height) (Rahli et al. 2011). This parameter has been found to have a great impact on this heat transfer mode. Hence, (H. K. Moffat 1988; H. Moffat and Jensen 1986) noticed that the structure of the secondary flow due to thermal instability is very sensitive to the channel aspect ratio A. In the case of a large transverse elongation ($A \geq 6$), the longitudinal rolls appear gradually in the duct: they are first initiated near the vertical walls and then spread progressively to the interior of the channel (Rahli et al. 2011). This parameter has been investigated by Combined flow visualization and temperature measurement (Chang and Lin 1998). Thus, Reynolds number was varied from 2.5 to 50, Rayleigh number from 3000 to 20,000 and the aspect ratio A from 2 to 12, covering the steady and unsteady longitudinal vortex flows. (Gau et al. 1999) achieved experimentations to investigate the effect of aspect ratio A (width to height) at the entrance of a channel of A=6.67. Reynolds number ranges from 100 to 2000 and the buoyancy parameter Ri from 2.5 to 907. In his paper (Ozsunar, Baskaya, and Sivrioglu 2001) [reports preliminary results of a numerical investigation of mixed convection heat transfer in horizontal and inclined channel (aspect ratio A=10), uniformly heated from below. Reynolds number was ranged from 50 to 2000 and Gr from $7x10^5$ to $4x10^6$

Since the process is very complex, the first numerical studies on mixed convection were in 2D because it was difficult to model the complex phenomenon. 3D numerical simulations of PRB (Poiseuille-Rayleigh-Benard) flows are relatively recent and not so numerous because computations of such flows necessitate large meshes and high computational costs. (Benzaoui, Nicolas, and Xin 2005) have presented and validated an efficient vectorized finite difference code to solve 3D incompressible Navier-Stokes equations under Boussinesq approximation for mixed convection flows in high aspect ratio channels. They dealt with steady longitudinal rolls, unsteady transverse rolls and for the first time, wavy rolls. With the development of CFD techniques (Bammou et al. 2013) used this powerful tool to resolve complex flow and visualize the roll development mechanism in mixed convection in details. (Rahli et al. 2011) have achieved numerical study of 3D laminar double diffusive mixed convection in horizontal rectangular ducts. Recently, some experimental studies based on latest visualization techniques of Particle Image Velocimetry (PIV) (Elatar and Siddiqui 2014) have investigated the effect of bottom wall heating on the flow structure inside a horizontal square channel at low Reynolds numbers (Re) and high Grashof numbers (Gr). The POD analysis revealed the presence of convective cells primarily in the lower half of the channel. In mixed convection flow, the heat transfer characteristics are different depending on whether the flow is developing or fully developed. Meyer and co-workers (Meyer and Everts 2018; Meyer et al. 2019; Everts and Meyer 2018) investigated thermal entrance length and Nusselt number in mixed convection regime and identified the existence of three different regions for developing laminar flow and proposed new correlations for mixed convection in the three regions.

Some of the above studies were summarized in table 1. This summary is of course no exhaustive and claims no completeness.

Authors	Re	A	Ra/Gr	Ri	Q	fluid	study	flow
Abou-Ellail83	275	A=1,4	/	/	/	Pr=4	Num	Thermal entry region
Incropera, Shutt 85	100-1000	A=1-10	$Gr=2.5x10^5$-$6.5x10^6$	/		Pr=6.5	Num	Entrance region
Maughan, Incropera 87	125-500	A=10	$Gr^*=7x10^5$-10^6	/	/	Pr=0.7	Exp	Thermal entrance region
Lin95	9-186	A=4	$Gr<5.10^6$		/	Pr=0.7	Exp	Fully developed
Chang 98	50-100	A=2-12	Ra=3000-20000			Pr=0.7		Thermal entrance region
Gau 1999	100-2000	A=6.67		2.5-907		Pr=0.7	Exp	Thermal entrance region
Oszunar 2001	50-1000	A=10	$7x10^5<Gr<4x10^6$	0.14-21.33		Pr=0.7	Num	Thermal entrance region
Abid 2006	Re=20	A=1.9	$Gr=4.3x10^5$-$4.2x10^6$			Pr=6	Exp	Fully developed
Benderradji 2008	0-100	A=10	$Ra=0$-10^6		0-200 W/m2	Pr=7	Num/exp	Fully developed
Rahli 2011	Re=50, 70	A=5,8,10	$Ra=5x10^3$			Pr=.7 Sc=0.14	Num	Fully developed
Taher 2018	25-150	A=10	Ra=104-107				Exp	Fully developed
Our study	Re=50-1000	A=10,15, 20,40	$Gr^*=6.87x10^2$ to $8.8\ x10^5$	$6.87x10^{-4}$ -351	200-1000 W/m2	Pr=0.7	Num	Thermal entrance region

Table 1 summary of some studies about aspect ratio effect in mixed convection flows

Most of those studies studied the effect of Aspect ratio in the range of A=1-12 but higher aspect ratios have not been examined. Furthermore, the range of parameters used was not extended enough. Based on this literature survey, our aim in this study is to extend the most important parameters that impact mixed convection in the particular case of upward solar air heater (SAH). SAHs are particular type of heat exchangers that convert solar radiation into thermal energy using air as working fluid. The most important applications of SAHs are space heating and cooling, and some industrial heat process like drying (Kalogirou 2004). SAHs can also be integrated with photovoltaic (PV) systems to produce both thermal energy and electricity, called PV/T collectors. SAHs may be classified according to number of air passes into single-pass and double-pass. In single-pass SAH, air flows in one way either above the absorber plate or below it. They are generally divided into two types:

- type I (Upward air pass) with air flowing between the absorber plate and the cover glazing;
- type II (Downward air pass) with air flowing between the absorber plate and the back panel;

There are several parameters impacting the solar air heaters efficiency: type and shape of absorber plate, number of glass cover plate, the use of artificial roughness (Yadav and Bhagoria 2013; Boulemtafes-Boukadoum 2014) or baffles. As it is described by (Hollands, K.G.T 1979), the collector geometry is one of the most important parameters to investigate in order to reduce convective losses. To reach high thermal efficiencies in SAHs, heat has to be transferred efficiently from the absorber to the flowing air. Several investigators have attempted to design more efficient solar air heaters by proposing appropriate design of SAH's air channel geometry. By theoretical analysis, (Altfeld, Leiner, and Fiebig 1988b; 1988a) demonstrated optimal air velocity corresponding to the channel depth in downward SAH (type II). Hegazy (Hegazy 1999) suggested a criterion ratio of depth to length as 0.0025 for SAH type II. (Gan 2009) performed CFD simulations to find the optimal air gap in Trombe wall and behind building integrated photovoltaic panels [35].

Most of above-mentioned design and optimization studies are limited to forced convection flows neglecting the effect of mixed convection. However, the air flow rate in some practical operating conditions of SAH is very low and vary widely due to solar radiation randomness. At low Reynolds number and under specific solar radiation, buoyancy effects are very high in upward solar air heater leading to the onset of thermo-convective instability and longitudinal rolls development. (Sun, Ji, and He 2010) carried out 2D CFD analysis to found out the optimum channel height of SAH type I (upward), and type III (double pass). The optimal channel depths for type I and type III SAHs with black-painted absorber are suggested to be equal to 10 mm in the range of investigated parameters of mass flow rates between 0.01 to 0.06 Kg/s, corresponding to Reynolds number of 500 to 4000. For the parameters investigated, Ri* is very low, inertia forces are higher than buoyancy forces and hence, the results obtained are comparable to that of forced convection flows. The analysis was based on first and second laws of thermodynamics and thus does not take into account the effect of mixed convection.

The aim of this study is to investigate 3D unsteady mixed convection air flow in Upward solar air heater under some specific parameters to approach the real operating conditions of SAH at low Reynolds numbers (50 to 1000). Our main objective is to extend mixed convection parameters range to large channel's aspect ratios (A= 10 to 40), various bottom wall heat flux (200-1000W/m^2) and to consider some additional effects, such as mixed heat boundary condition on the top wall (glazing). Since channel's height (Aspect ratio) is a principal variable to be fixed in the design of solar air heaters (SAHs), we emphasize on the influence of channel height on the flow structure and heat transfer augmentation using Computational Fluid dynamics (CFD) techniques.

Combined flow visualizations and heat transfer calculations are carried out to investigate all these parameters in a large range of Grashof number ($6.87x10^2$ to $8.8x10^5$) and Richardson number Ri*($6.87x10^{-4}$-351) covering forced, natural and mixed convection of steady and unsteady air flows.

2. Model and Numerical procedures

As depicted in Fig.1, 3D mixed convection air flow in upward solar air heater was numerically analyzed. The physical domain consisted in cross section rectangular channel (LxWxH) heated from below. The top wall (glazing) is subjected to external heat losses: convective heat transfer with ambient and radiative heat exchange with the sky. Conductive heat transfer into glass thickness (e_v) has been taken into account using SHELL CONDUCTION option of ANSYS Fluent code. The bottom wall (absorber)is submitted to Constant Heat Flux (CHF) (as received solar radiation). The lateral walls are considered adiabatic.

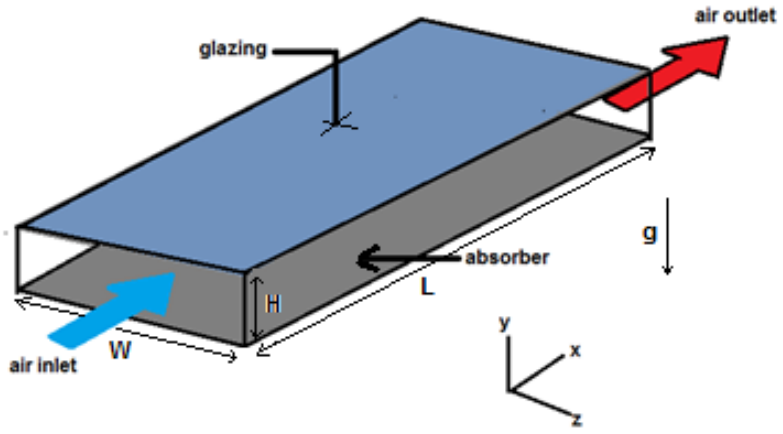

Fig.1 Schematic view of the computational domain

The channel's dimensions are:
Ox, L= 100 cm; 50 cm
Oy, H=0.5 to 2 cm
Oz ; W=20 cm
Glass thickness e_g= 3 mm
Spanwise Aspect ratio (A=W/H= 10 to 40)

The working fluid (air, Pr=0.7) is laminar, transient and governed by unsteady Navier-Stokes equations. It is assumed that the fluid is Newtonian and incompressible with constant thermo-physical properties except in the term of density. Buoyancy force is expressed by Boussinesq approximation and thermal radiation is neglected except in the heat exchange between the glazing and the sky. The viscous dissipation and compressibility effects in the energy equation are neglected. The fundamental equations used to determine the velocity , the pressure and the temperature were the continuity, Navier-stokes equation and the energy equation. According to he foregoing assumptions, the governing equations with reference to Cartesian coordinates *x, y, z* are:

Mass conservation

$$\frac{\partial u}{\partial x}+\frac{\partial v}{\partial y}+\frac{\partial w}{\partial z}=0 \qquad (1)$$

Momentum conservation

$$\frac{\partial u}{\partial t}+u\frac{\partial u}{\partial x}v\frac{\partial u}{\partial y}+w\frac{\partial u}{\partial z}=-\frac{1}{\rho}\frac{\partial P}{\partial x}+\nu\left(\frac{\partial^2 u}{\partial x^2}+\frac{\partial^2 u}{\partial y^2}+\frac{\partial^2 u}{\partial z^2}\right)+g\beta(T-T_o)\cos\theta \qquad (2)$$

$$\frac{\partial v}{\partial t}+u\frac{\partial v}{\partial x}v\frac{\partial v}{\partial y}+w\frac{\partial v}{\partial z}=-\frac{1}{\rho}\frac{\partial P}{\partial y}+\nu\left(\frac{\partial^2 v}{\partial x^2}+\frac{\partial^2 v}{\partial y^2}+\frac{\partial^2 v}{\partial z^2}\right)+g\beta(T-T_o)\sin\theta \qquad (3)$$

$$\frac{\partial w}{\partial t}+u\frac{\partial w}{\partial x}v\frac{\partial w}{\partial y}+w\frac{\partial w}{\partial z}=-\frac{1}{\rho}\frac{\partial P}{\partial z}+\nu\left(\frac{\partial^2 w}{\partial x^2}+\frac{\partial^2 w}{\partial y^2}+\frac{\partial^2 w}{\partial z^2}\right) \qquad (4)$$

Energy conservation

$$\frac{\partial T}{\partial t} + u\frac{\partial T}{\partial x} v\frac{\partial T}{\partial y} + w\frac{\partial T}{\partial z} = a\left(\frac{\partial^2 T}{\partial x^2} + \frac{\partial^2 T}{\partial y^2} + \frac{\partial^2 T}{\partial z^2}\right) \quad (5)$$

Uniform air flow at the channel's entrance ($u=u_0$, v=0, w=0), atmospheric pressure at the outlet and non-slip condition on the walls are the hydrodynamic boundary conditions applied to the studied domain. Thermal conditions applied are:

$T=T_i=T_{amb}$ at the inlet

mixed boundary condition was applied on the glazing (top wall) :

$Q_g=h_w(T_g-T_{amb})+\varepsilon\sigma(T_g^4- T_s^4)$ (6)

With T_s, the sky temperature calculated by Swinbank expression [37]:$T_s= 0.0552 * T_{amb}^{1.5}$ (7)

on the absorber: Constant heat flux imposed Q_{abs}=200 to 1000 W/m^2

lateral walls: they are considered adiabatic with zero heat flux, q=0

Simulations parameters used to investigate the effect of channel's height on flow patterns and heat transfer in mixed convection airflow are:

Q_{abs}=200 to 1000 W/m^2

Re =50 to 1000

Gr*= 6.87x10^2 to 8.8 x10^5

Ri*=Gr*/Re^2= 6.87x10^{-4} to 351

Since this is a PRB flow study and as the major scientific works in this area, Reynolds number and modified Grashof number were calculated using H as characteristic length:

$$Re = \frac{UH}{\nu} \quad (8)$$

$$Gr^* = \frac{g\beta Q H^4}{k\nu^2} \quad (9)$$

To estimate heat transfer we have calculated the local Nusselt number by

$$Nu(x) = \frac{h(x)D_h}{k} \quad (10)$$

$with\ h(x)$local convective heat transfer coefficient expressed by :

$$h(x) = \frac{Q}{T_{p(x)} - T_{b(x)}} \quad (11)$$

3-Numerical resolution

Considering the nonlinearity in the inertia terms of fundamental equations, they were solved numerically using a CFD(Computational fluid dynamics) code FLUENT 14.5 (ANSYS), based on finite volumes method (FVM).

Second order Upwind scheme was used to discretize momentum and energy equations. Pressure was interpolated using PRESTO! scheme. We used PISO algorithm to handle the

pressure-velocity coupling. Time advancement was carried out using First order implicit scheme.

Due to the iterative process of numerical resolution, convergence was used as the monitor of final solution achievement. Convergence was considered as being completed when residuals become less than 10^{-5} for the velocities and 10^{-7} for energy for most of the cases tested. Visualization and calculations of some averaged variables were performed to confirm the convergence. As depicted in Fig.2, temperature contours on the absorber is stable after almost 2000 to 3000 iteration in the steady state. (Case H=1cm, L=1m, Q=600W/m^2, Re=50).

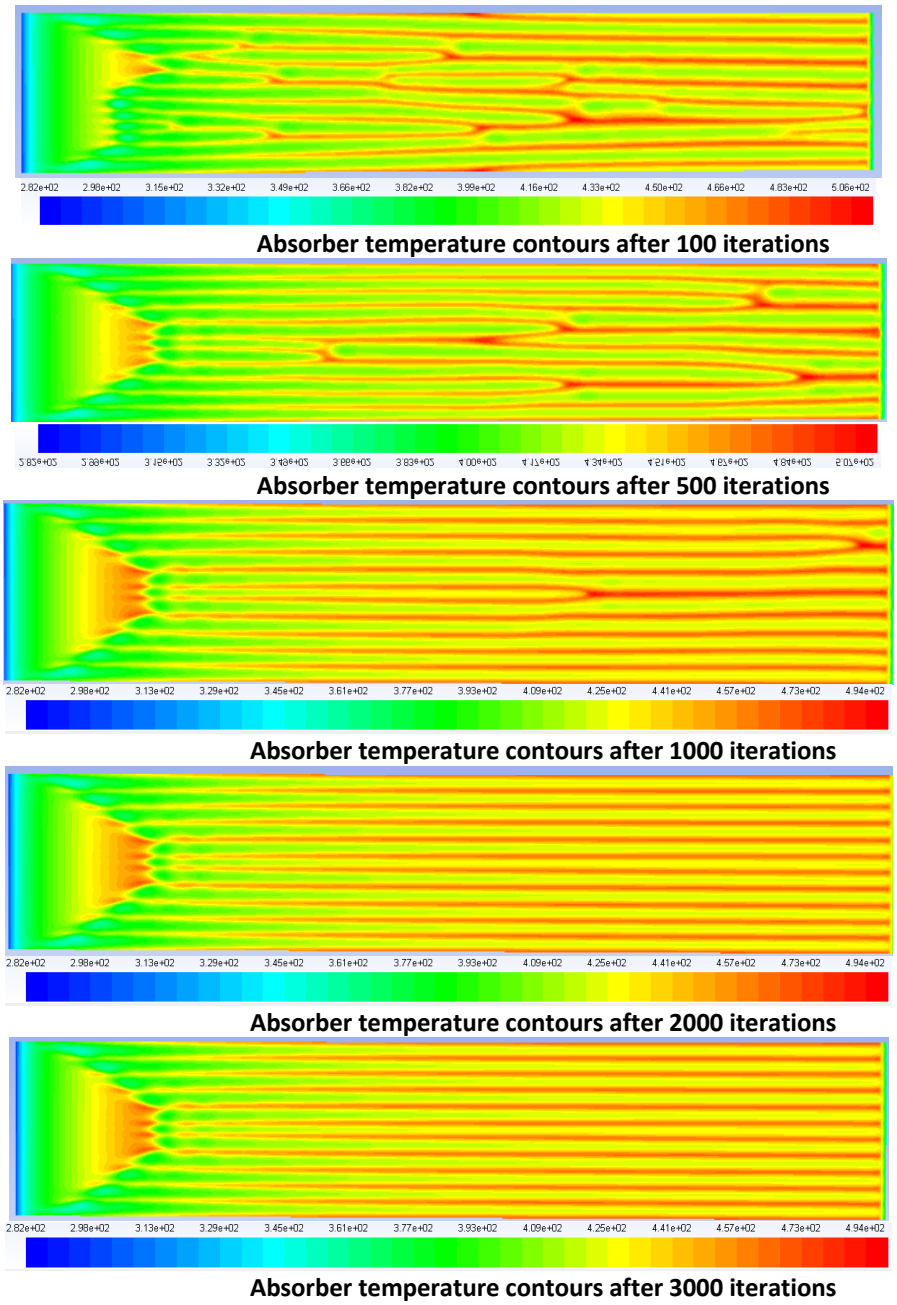

Fig.2 Temperature contours for different iteration numbers

Grid independence checking

Velocity and temperature gradients are very important near the walls. Hence ,the generated grids were very dense near the walls. The meshes applied to the solution domain are structured and non-uniform with a refining near the walls. For L=1m, grids size vary from 530.000 to 2 400 000 cells depending on channel's height.

Several grid sizes have been tested to ensure that the results are grid-independent. The appropriate mesh size is the one who gives the best compromise between accuracy and calculation cost.

The results of test grid performed for the case of L=1m, H=1cm, Re=50, Q=600W/m^2 are presented below.(G1=135000 cells, G2=880 000, G3= 1 116 000 to G4=2340 000). In Fig.3, is depicted T_{abs} evolution along the channel for the four grid meshes. We can observe that from the grid of 1116000 there is no noticeable difference. Thus G3 was selected to balance the computational load and the numerical accuracy.

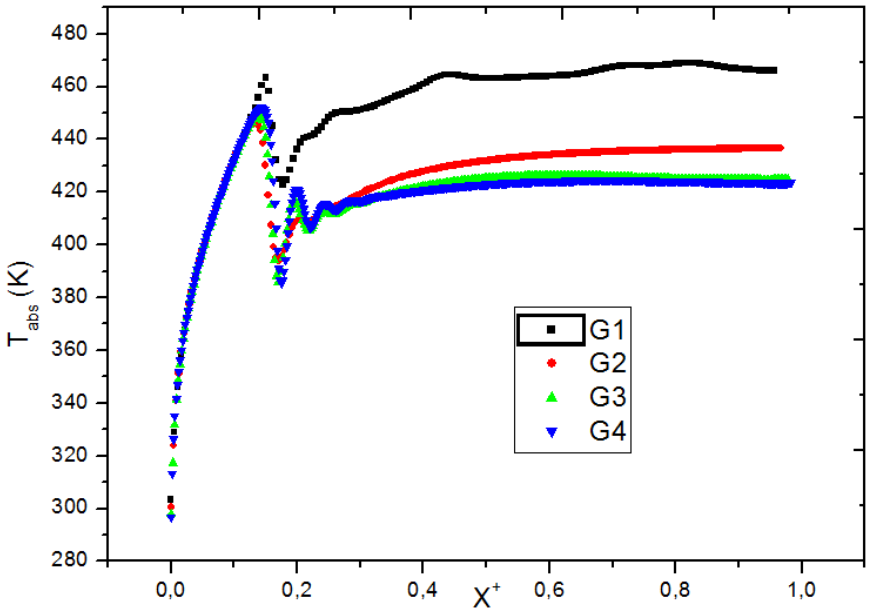

Fig.3Local absorber temperature evolution along the channel (z=0.1) obtained with four mesh grids

Temperature contours on the absorber for each grid are shown in Fig.3. One can observe that the flow structure is stabilized from G3 grid.

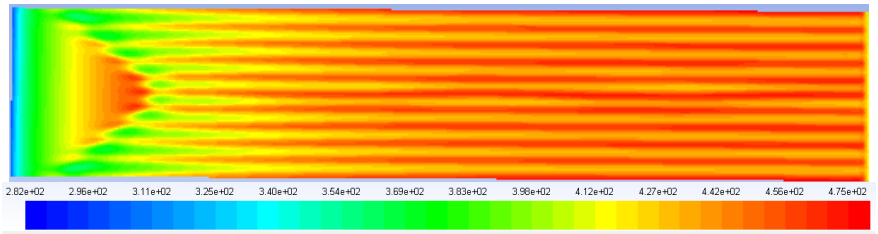

Absorber temperature contours with 135000 cells (G1)

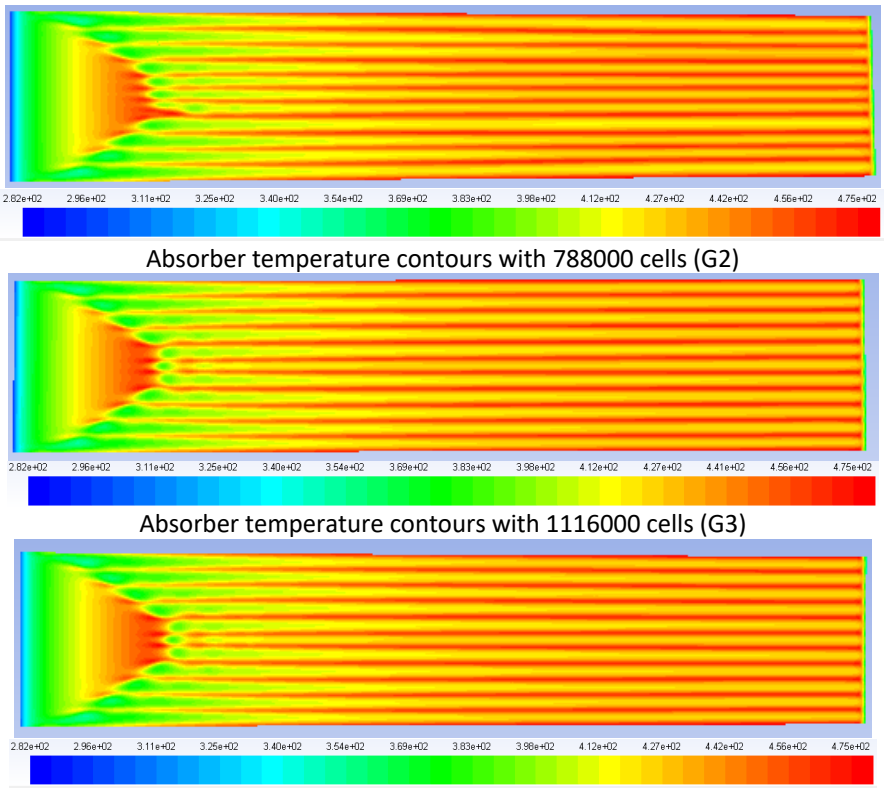

Fig.4 Temperature contours on the absorber obtained for Four (04) different grid sizes

Validation case

The model validation was performed for the case of forced convection air flow in a rectangular channel heated from below studied by (Maughan and Incropera 1987) as shown in Fig.5. As predicted by theory, Nusselt number decrease quickly to reach an asymptotic value as expected for the case of pure forced convection. We can observe that our predicted longitudinal Nusselt number variations agree well with experimental results of Maughan.

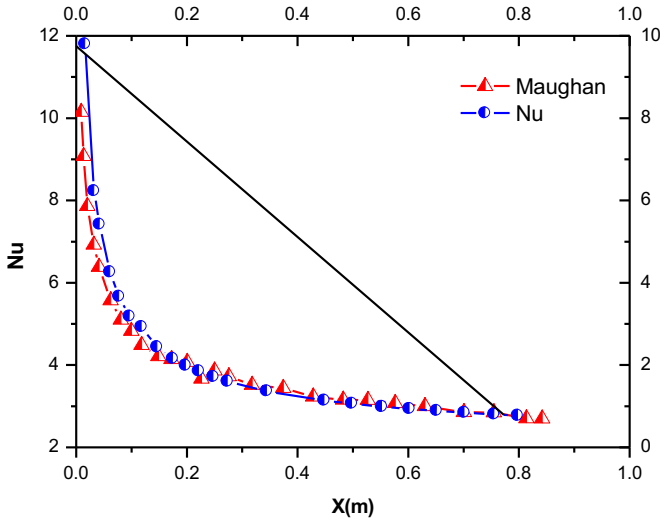

Fig.5 Comparison of Nusselt number longitudinal distribution in the case of forced convection

In the case of mixed convection, the reliability of our numerical results was verified by comparing them to data reported in literature: numerical solution of (Ozsunar, Baskaya, and Sivrioglu 2001) and experimental data of (Maughan and Incropera 1987). The present results are related to the case of $Gr^*=2.10^5$, Re=250, A=10.Fig.6 shows Nusselt number longitudinal variation in the flow direction. In mixed convection Nu decrease to the minimum then it start to increase to a maximal value before reaching the asymptotic value . This mechanism will be explain in details in the following results. This comparison has showed that our numerical predictions are much closer to experimental results of Maughan than those of Oszunar. This can be explained by the fact that we have used different CFD codes with different simulations parameters. Also, Oszunar has not used Boussinesq approximation and considered that air density is dependent of temperature only. Notice that in figure 5 and 6, Nusselt number was calculated using H as characteristic length to follow Maughan results.

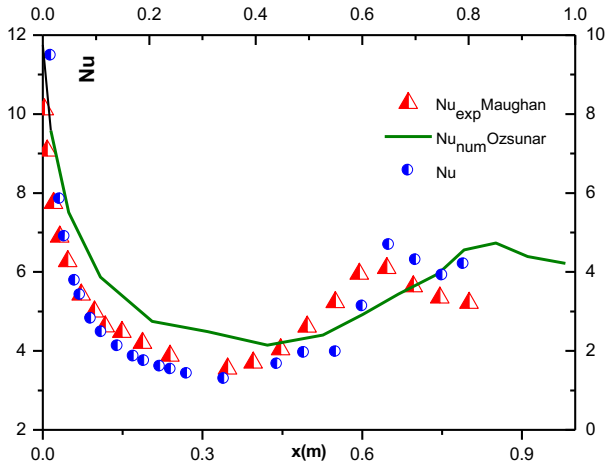

Fig.6 Comparison of Nusselt number longitudinal distribution in the case of mixed convection ($Gr^*=2.10^5$, Re=250, A=10)

3. Results and Analysis

All computations were carried out for air flow (Pr = 0.71) in a rectangular channel of large aspect ratio A=10 to A=40, with Reynolds number varying from 50 to 1000.The modified Grashof number varies from $6.87x10^2$ to $8.8\ x10^5$ and consequently the buoyancy- to-inertia ratio variation is within a wide range from very low to very high values.

In the present three-dimensional unsteady flow simulations, a large number of results data were obtained. Only a few of these results will be presented here (L=100cm, θ°=0) for horizontal channel to mainly explain the effects of various parameters on the characteristics of mixed convective flow patterns and heat transfer in the particular case of upward solar air heater.

Preliminary investigation of flow pattern

Forced convection

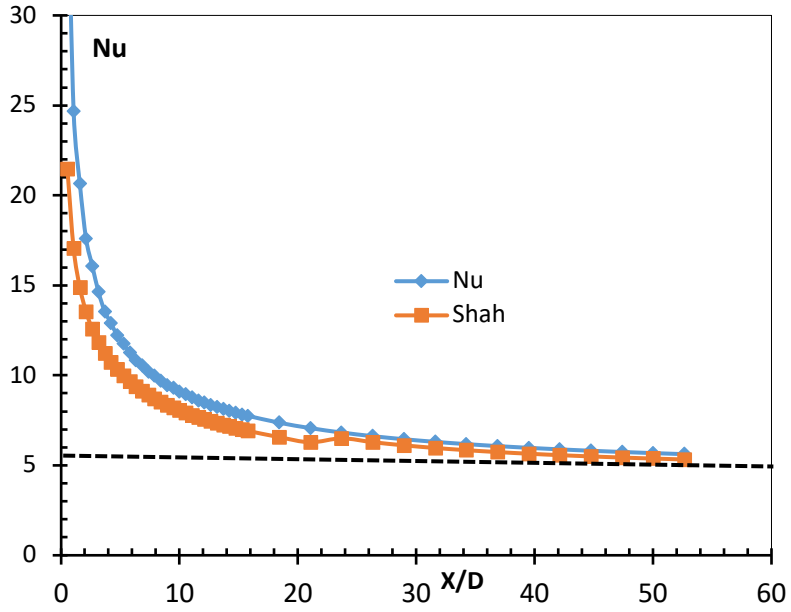

Fig.7 Nusselt number variation along the channel for the case of pure forced convection (A=20, Re=1000, Q=600W/m^2)

Fig.7 depicts Nusselt number variation in the longitudinal direction for H=1cm (A=20), Re=1000, Q=600W/W/m^2. In this case Gr*=3,30x10^4 and Ri*=0.032 which verifies the conditions of pure forced convection. After a quick decrease, Nu reaches the asymptotic value of 5.61 which is close to the theoretical value of 5.39 for the case of parallels plates with one plate heated for fully developed laminar flow (Meyer and Everts 2018). Is also plotted the correlation of (R.K. Shah and A.L. London 1978) for simultaneously thermally and hydrodynamically developing flow. Fig.8 shows local Nusselt number as function of the inverse of Graetz number. Local Nusselt number at different heat fluxes is presented in Fig.9. As expected, there is no significant difference between the four heat fluxes, which confirms that is pure forced convection flow.

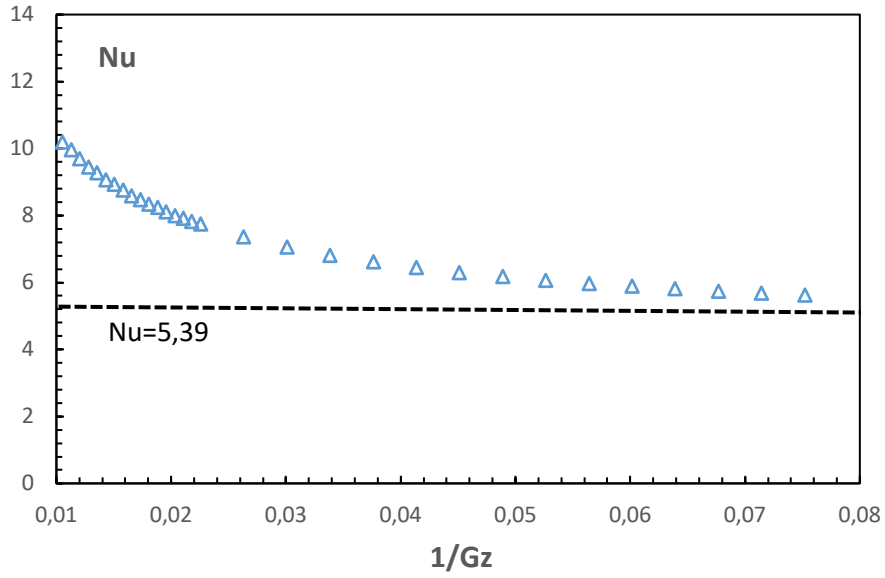

Fig.8 Nusselt number as function of the inverse of Graetz number for (A=20, Re=1000, Q=600W/m^2)

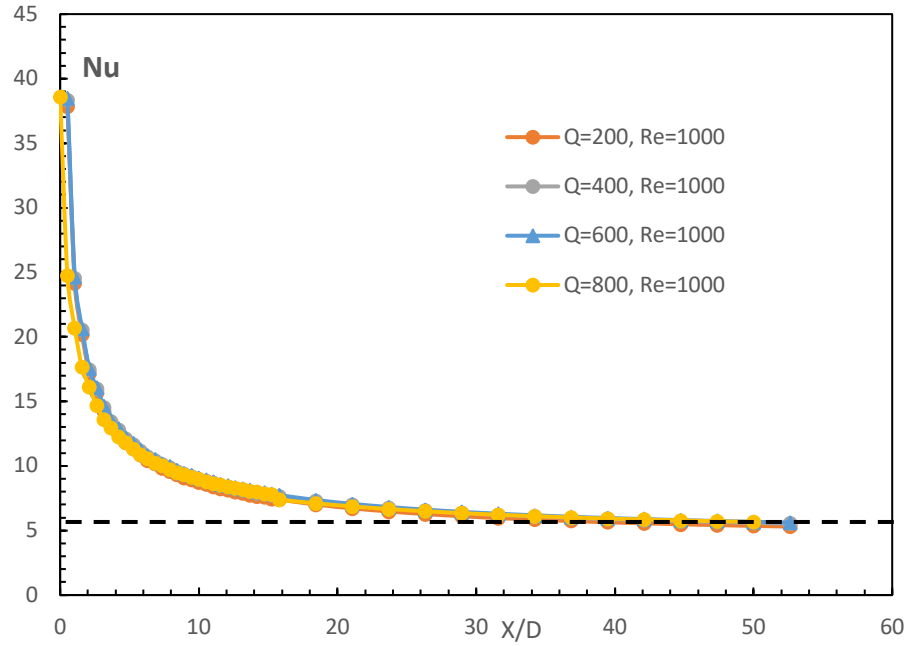

Fig.9 Forced convection Nusselt number for different heat fluxes (A=20, Re=1000, Q=600W/m^2)

In Fig. 10, the curve of spanwise-averaged longitudinal Nusselt number of mixed convection laminar flow in rectangular channel of H=1cm (A=20). The modified Grashof number *(Gr* =* 3.3 x 10^4 , Ri*=13.19) is calculated on the base of the generated flux and the inlet conditions. In forced convection region, the Nusselt number's curve shows a monotonic decrease as in the case of pure forced convection flow. Then, as buoyancy forces become strong enough to destabilize the boundary layer, one can observe the onset of the instability characterized by a rise of the local spanwise-averaged Nusselt number [9].

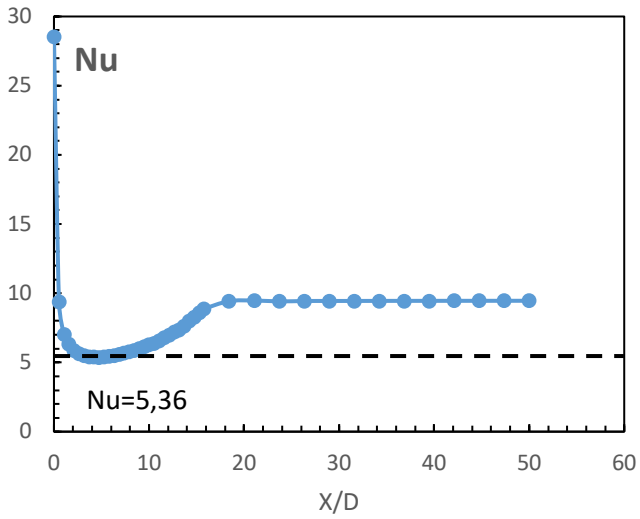

Fig.10 Spanwise averaged longitudinal distribution of Nusselt number for the case of mixed convection (A=20,Q=600W/m^2, Re=50)

After the onset of the instability, ascending plumes of warm fluid growth along the side walls from the heated surface. Thus, the bottom plate is cooled by fresh fluid descending from the core of the channel to the plate. This secondary flow is a strong mechanism to heat transfer enhancement. This is the region of mixed convection, where Nusselt number is highly enhanced depending on Grashof and Reynolds numbers. Toward the channel exit, the amplitude of variations in Nusselt number decrease to reach a stable shape. The mechanism of roll development is well illustrated in Fig.11, where are plotted the contours of local temperature on the absorber (bottom heated plate) and also in Fig.12 where are shown the contours of both temperature and velocity longitudinal component u in different cross sections along the channel.

At x=0.01m, the flow is in laminar forced convection regime characterized by vertical temperature gradient and parabolic shape of velocity's contours.

As the flow moves downstream, the boundary layer at the bottom wall becomes thicker and the temperature is higher. This leads to the rise of longitudinal rolls near the side walls (x=0.15m). This is confirmed by the contours of u velocity that exhibits a distortion at the same locations.

Then at x=0.3m more longitudinal rolls are induced but the fluid's core is still not destabilized yet and rolls number increase in pairs to reach the fully developed state and their maximum number (20) at x=0.45 m. Here, the roll's height and lateral extension are higher as observed by (Gau et al. 1999). This length where the rolls invade the whole cross section corresponds to the establishment (development) length and it will be noted Le. At the channel exit, the roll size is approximately equal to the channel's height (Benderradji et al. 2008) .The rolls can be identified in both temperature and velocity contours. Fig.12 depicts 3D contours of temperature, and velocity for the case (A=20, Re=50, Q=600W/m^2).

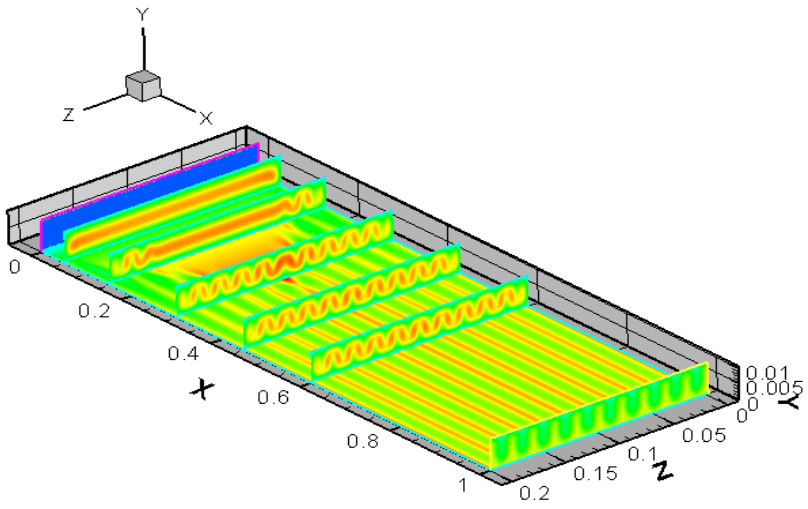

Fig.11 Temperature contours on the absorber plate (H=1cm, Q=200W/m^2,Re= 50)

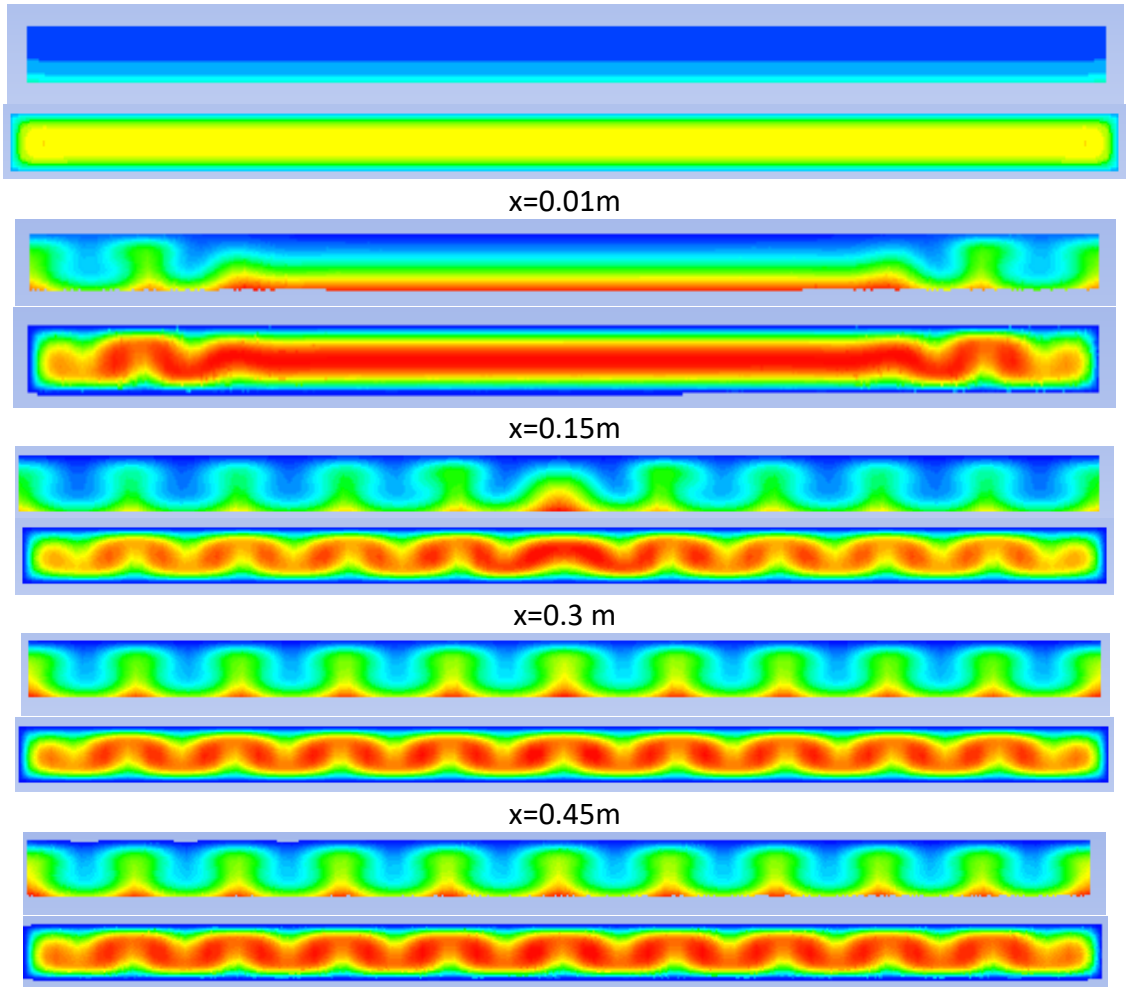

x=0.01m

x=0.15m

x=0.3 m

x=0.45m

x=0.6m

Fig.12 Temperature and U velocity contours at different cross sections of the channel

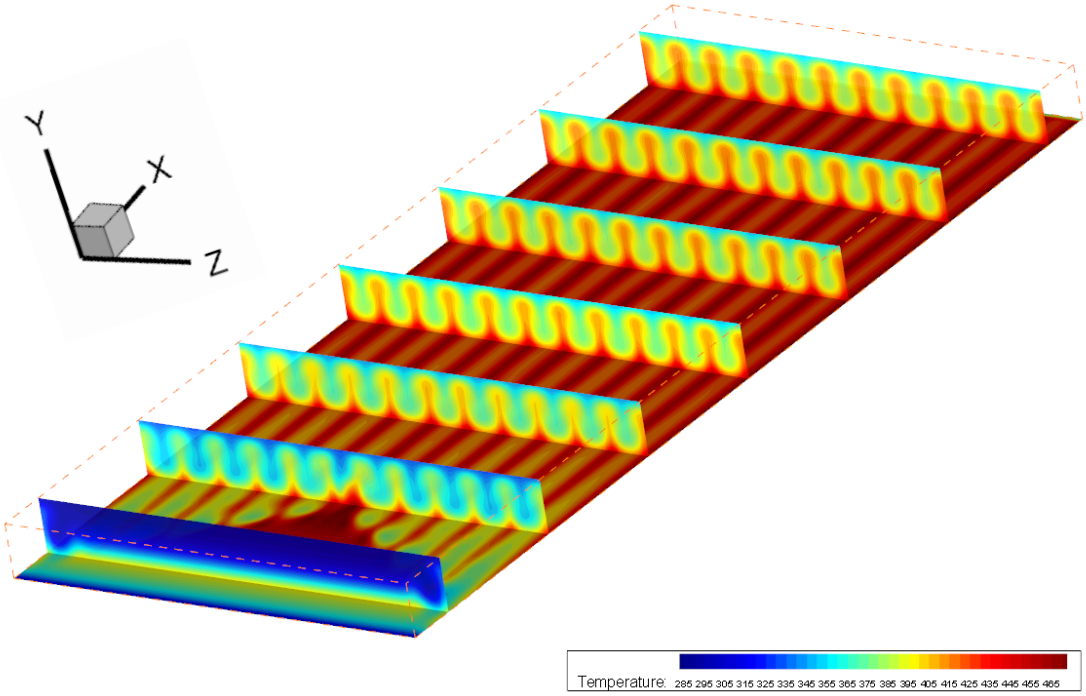

a) Temperature contours

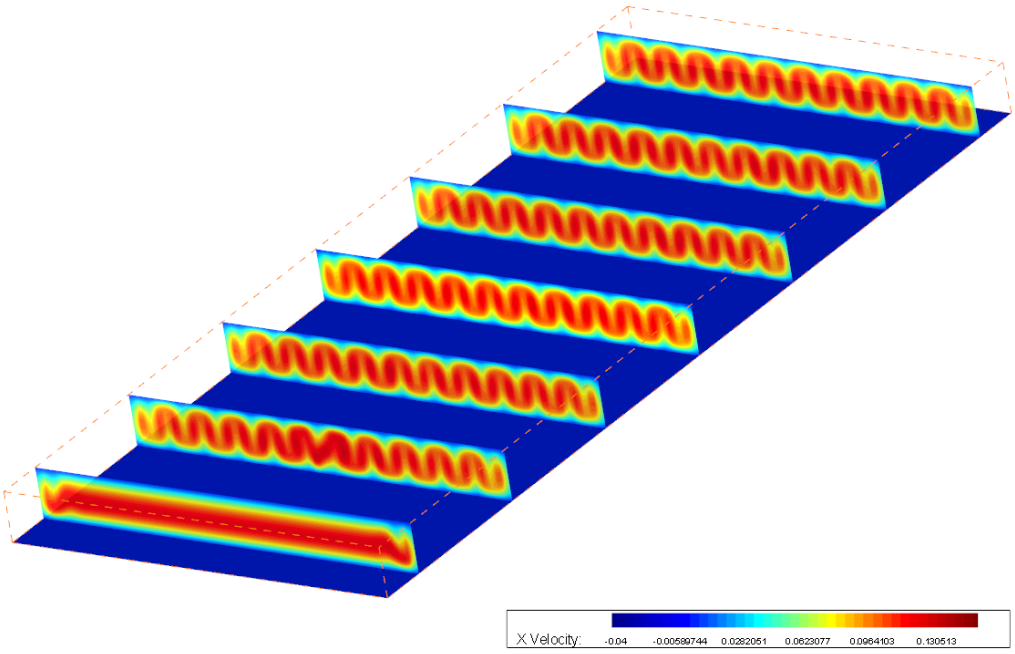

b) Contours of velocity component in the x direction

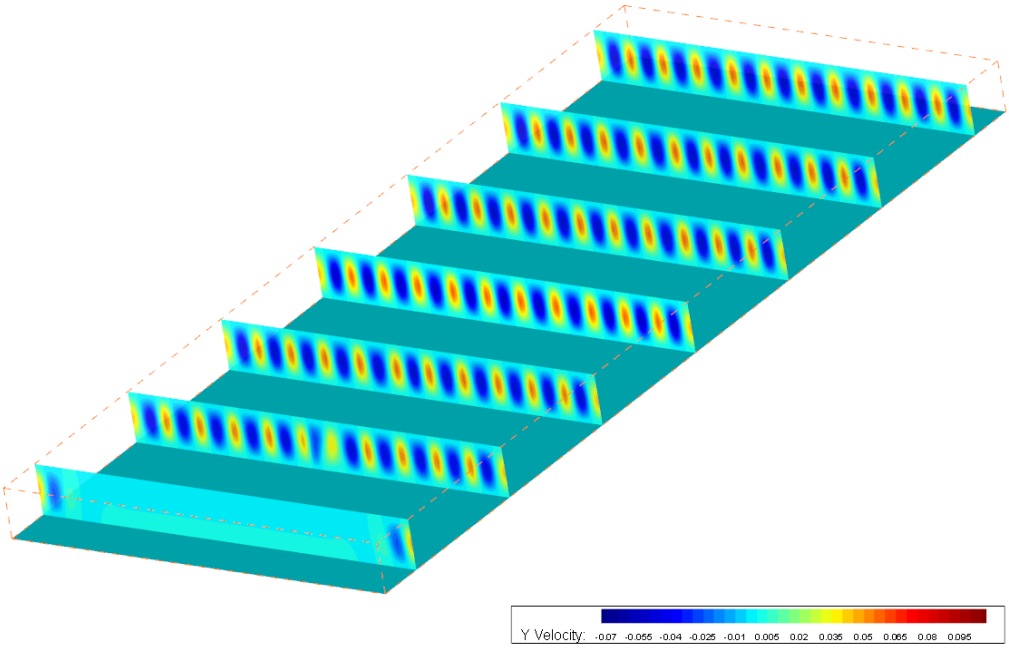

c) Contours of velocity component in the y direction

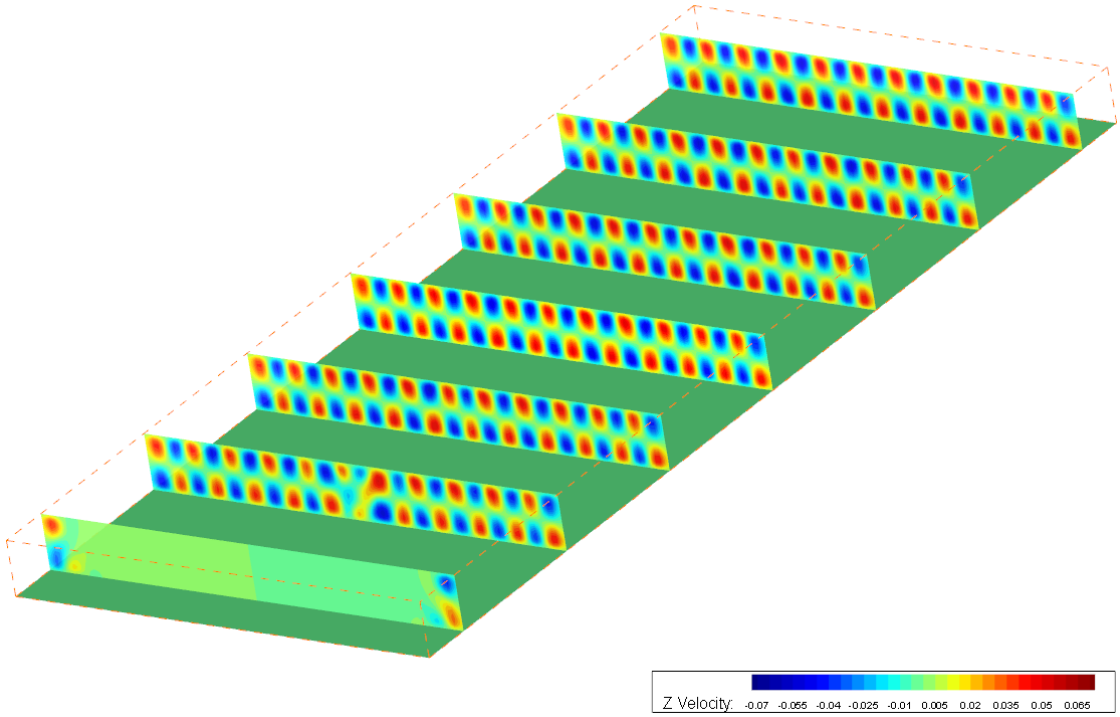

d) Contours of velocity component in the z direction

Fig.13 3D Temperature and velocity contours at different cross sections of the channel (A=20, Re=50, Q=600W/m2)

3-1 Effect of heat flux supplied to the absorber (effect of Grashof number)

To examine the influence of Grashof number on rolls generation and temperature distribution, we varied the heat flux from 200 to 1000 W/m^2. Fig.14 shows the temperature contours as visualized by ANSYS code for the case of H=1cm, A=20, Re=50.

The main observations are that as heat flux increases, more rolls are induced and development length Le decreases as noticed by many authors (Benderradji et al. 2008; Gau et al. 1999). The longitudinal rolls are induced by the first roll initiation mechanism: rolls are primary initiated at the sidewalls of the channel and then they spread gradually to the flow's core in the downstream direction as already observed by previous authors. As heat flux increase (Q=600 w/m^2, Ri*=13.19), buoyancy forces are higher and the boundary layer at the heated wall becomes thicker. Hence, rolls initiation occurs at a much earlier stage and more rolls are induced (Incropera, Knox, and Maughan 1987). Nevertheless, these rolls are parallel and stationary. Such, the establishment length is shifted towards the channel inlet. When Q=800W/m^2 (Ri*=17.59), the number of induced rolls is again increased and one can notice a rolls destabilization so that several dislocations are observed. The development to unsteady state is more highlighted when the heat flux is more important (Q=1000W/m^2, Ri*=22.26). The flow structure evolves versus the longitudinal direction from laminar forced convection, laminar mixed convection, transitional and finally turbulent.

To examine locally the effect of heat flux on the roll development for different channel's height, we have plotted temperature (Fig. 13) and u velocity contours (Fig.14) at the same location (x=0.25 m) for five various heat flux values to highlight the effect of heat flux on the flow structure and roll development.

The temperature contours indicate clearly that for Q = 200 W/m^2, the flow's core is still dominated by forced convection and longitudinal rolls induced by side walls effect have a mushroom shape as described by (Gau et al. 1999). At Q=400 W/m^2, more longitudinal rolls are induced in the flow's core. For higher heat fluxes (Q=600, 800, 1000 W/m^2), corresponding to a higher Ri*, one can observe that the longitudinal rolls in the central zone develop simultaneously at the lower wall. These central rolls, referred as thermal plumes by (Gau et al. 1999), are initiated by the supercritical vertical thermal gradient at the lower wall (similar to Rayleigh–Benard instability). This is the second mechanism of roll initiation highlighted by (Benderradji et al. 2008) .

Also, one noticed that the number of rolls produced is proportional to Grashof number as reported in the literature (Gau et al. 1999), (Rahli et al. 2011), (Incropera et al.1987).

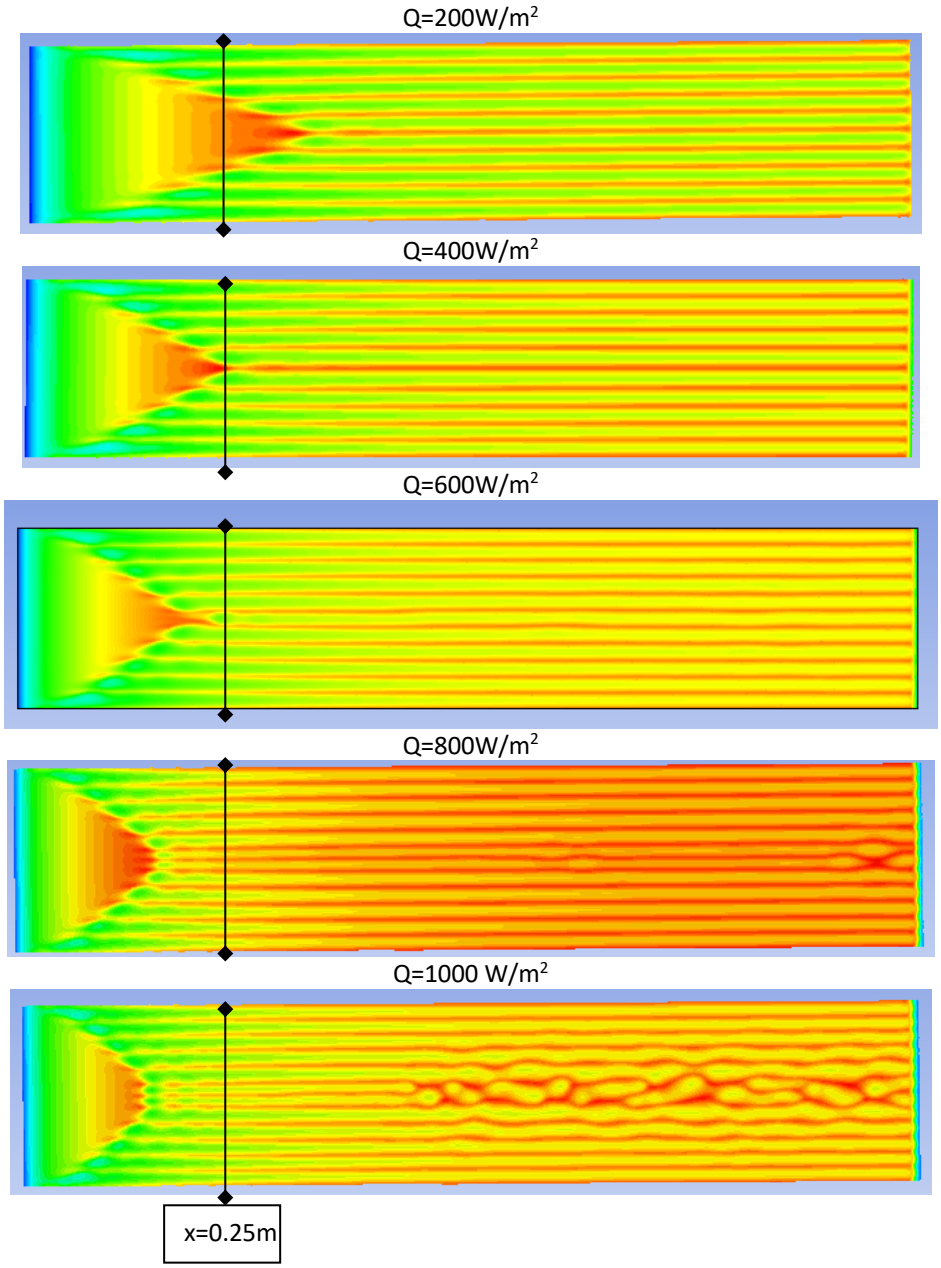

Fig.14 Longitudinal roll structures induced by various heat flux supplied to the absorber plate (H=1cm, Re=50)

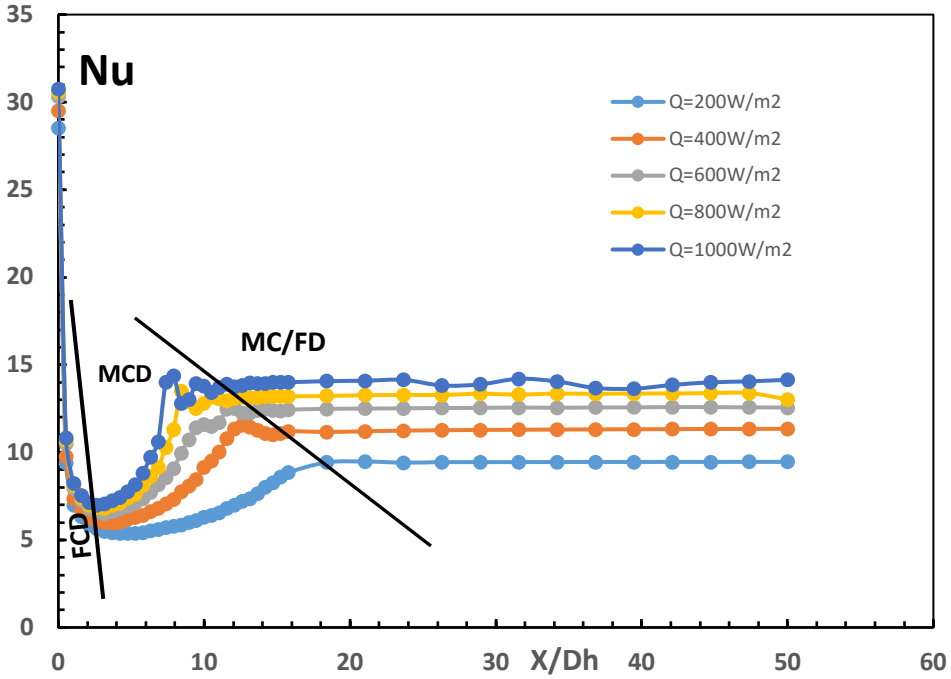

Fig. 15-a) Nusselt number longitudinal distribution for H=1cm (A= 20), Re= 50

Fig.15-a) depicts the spanwise-averaged longitudinal Nusselt number distribution for different values of heat flux (Q=200-1000 W/m^2) corresponding to Grashof number of (1.1 to 5.5x10^4). First, as expected, the maximum Nusselt numbers are close to the inlet where thermal boundary layer is thinner (Meyer and Everts 2018). For all the curves, Nusselt number decrease near the inlet, secondary flow effects are very small and Nusselt number variation is close to that of forced convection. With the increase of heat flux and consequently the Grashof number, the point where the onset of instability occurs is moved towards the channel inlet and secondary flow effects become larger. This effect is due to an increase in the thermal boundary layer thickness and temperature gradient that accelerate development of secondary flows (Maughan and Incropera 1987). The onset of instability in the flow is very fast, resulting in large fluctuations in Nusselt number values and thus higher enhancement in the heat transfer is obtained. Consequently, at the same Reynolds number, with increasing heat flux, instability occurs earlier and faster and Nusselt number is higher (Ozsunar, Baskaya, and Sivrioglu 2001) .

These observations agree well with (Meyer and Everts 2018) who reported that for mixed convection flow in circular ducts, the entrance length decreases when thermal effects are high enough. As reported by (Maughan and Incropera 1987), Nusselt number for each surface heat flux appears to approach a final asymptotic value, suggesting the existence of a fully developed condition. This is confirmed experimentally by Meyer and al for mixed convection in circular ducts. The authors describe 3 regions with different transfer mechanism: the Leveque region where Nusselt number decrease due to thermal entrance effects (FCD) to reach its minimal value where free convection and entrance effects are balanced. In region2, Nu is increasing due to buoyancy forces (MCD) before reaching the

asymptotic value where mixed convection is in fully developed (MCD/FD). These 3 regions are well identified in Fig.14-a)

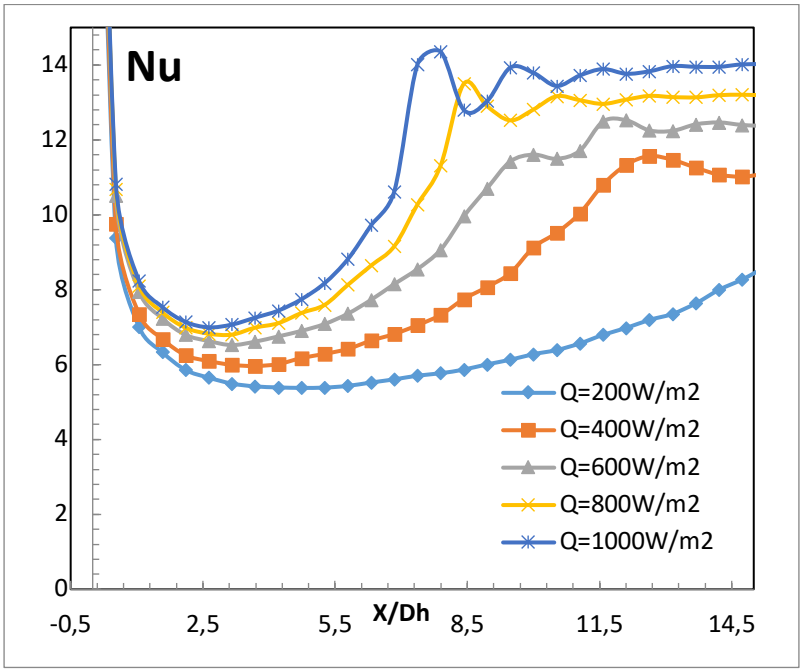

Fig. 15-b) Zoom on the region of instability onset

In Fig. 15-b), one can notice that for larger Grashof numbers, there is a noticeable departure in Nusselt number's curve from the forced convection zone before reaching the minimum as observed by (Maughan and Incropera 1987). Rapid boundary layer growth in this upstream region prevents the secondary flow from fully compensating for the effect of the thickening boundary layer. Hence, Nusselt number, although enhanced above the forced convection limit, continues to decline. An additional contribution to heat transfer enhancement in this region may come from an induced streamwise pressure gradient (Maughan and Incropera 1987) .

3-2 Effect of channel's height (Aspect ratio)

Results presented on Fig.16 exhibit the effect of the channel's height on the flow pattern for typical case of Re=50 and Q=200W/m^2. The channel' height varies from 0.5cm to 2cm corresponding to aspect ratio A= 40 to 10. In this case, even if heat flux is the same, modified Grashof number which is very sensitive to height (α to H^4) changes widely from 6.87x10^{2}to 1.76x10^5. In previous works, comparison were performed for two aspects ratio channels for the same Grashof number. In this study, we have decided to keep heat flux constant accordingly to real operating SAH under solar radiation. The goal is to find the optimal height for the same solar radiation.

For H=0.5cm, the flow looks to be entirely in forced convection regime because the buoyancy to inertia ratio is low (Ri*=0.27). For H=1cm, Ri* is more important (Ri*=4.39), the onset of instability occurs close to the inlet and the roll length development is approximately reached at X=0.35cm. As the value of the channel's height increases (H=1.5cm, Ri*=22.26), the point of instability onset is shifted toward the channel's inlet and the number of rolls

decreases as expected. For higher value of the channel's height (H=2cm), the buoyancy to inertia ratio is very high (Ri*= 70.36) and the longitudinal steady roll structure is destroyed, the regime is turbulent. Consequently, increasing channel's height enhances rolls induction and decreases development length but beyond a certain value, the regime becomes first chaotic and then turbulent. So, reducing the duct's height can stabilize the flow. As reported by (Rahli et al. 2011), the aspect ratio has an effect on the developed rolls number. This number is even despite the value of A.

On Fig.17 and Fig.18, we have plotted the temperature and u velocity distribution in a cross section at x=0.3m. One can see that for H=0.5 cm, there is no rolls and the flow seems entirely in forced convection regime. At H=1cm, the temperature and U velocity contours show that the length roll development is not reached yet. When the channel height increases (H=1.5cm), one can notice that the cross section of the rolls increases and their number decreases. The rolls structure symmetry is destroyed for H=2cm.

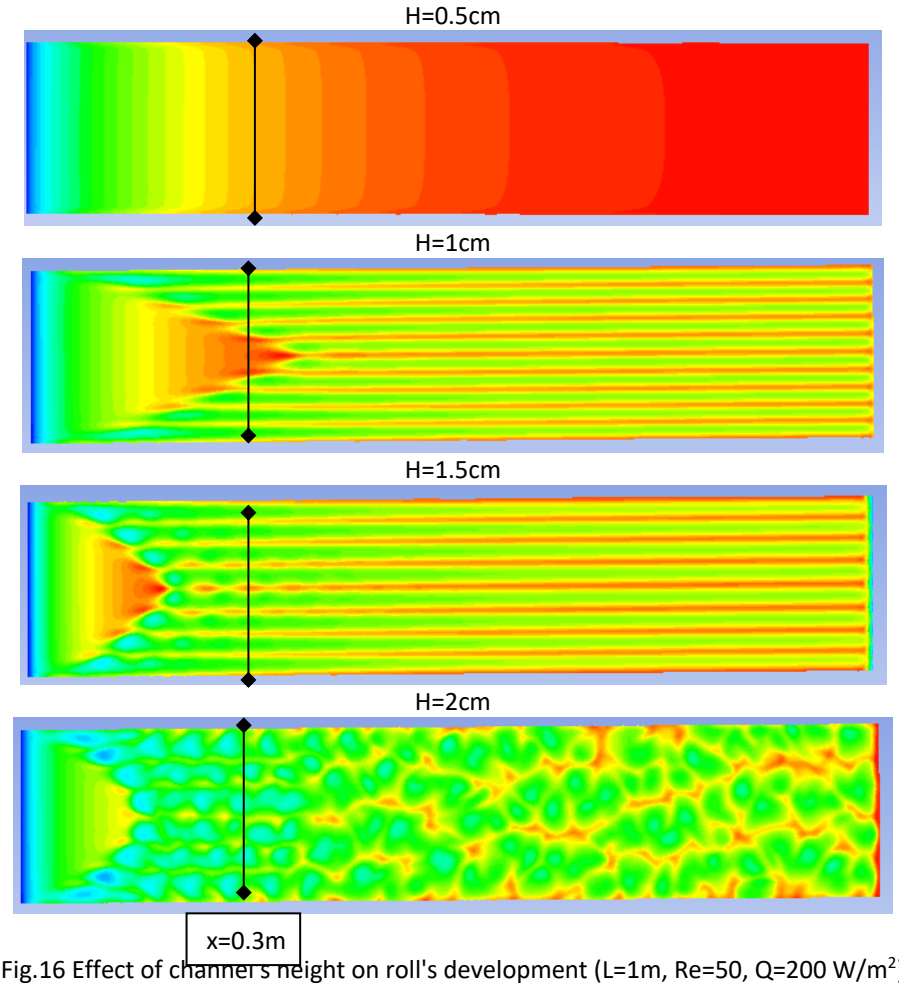

Fig.16 Effect of channel's height on roll's development (L=1m, Re=50, Q=200 W/m^2)

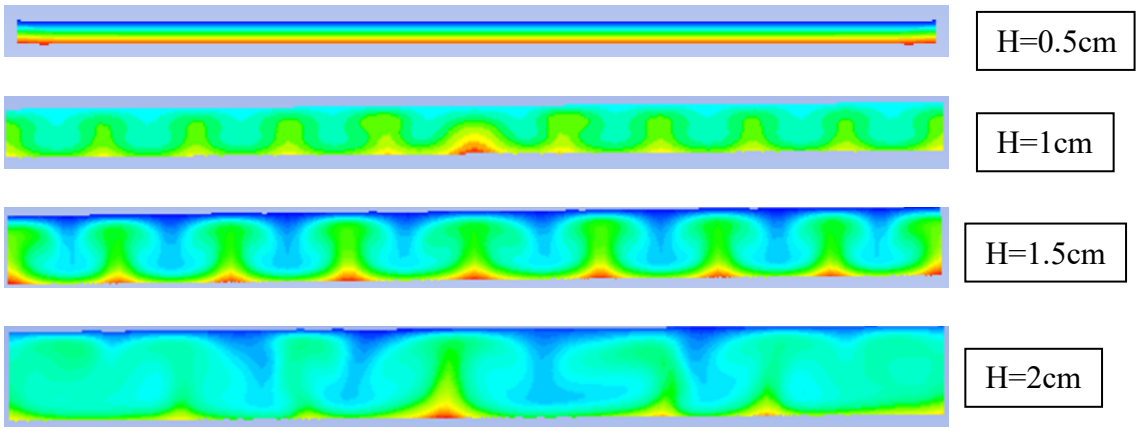

Fig. 17 Temperature contours for a cross section at x=0.3m

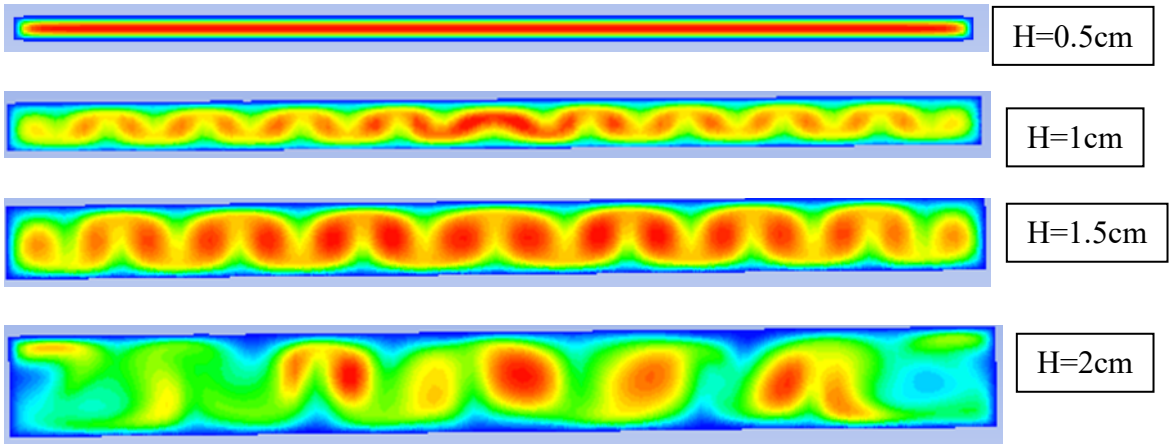

Fig. 18 U velocity contours for across section at x=0.3m

To highlight the effect of channel's height on heat transfer, we have plotted longitudinal spanwise-averaged Nusselt number distribution versus the longitudinal position in Fig.19.
One can observe that near the inlet, all the curves show the same decrease rate corresponding to the forced convection developing region. At low channel's height, the curve shape is analogue to that of forced convection regime. As the buoyancy forces increase, the Nusselt number raises rapidly to reach its maximum value related to heat transfer enhancement before reaching an asymptotic value (H=1cm). For H=1.5cm and H=2cm, the modified Grashof number is very high, consequently Nusselt number increases with channel's height increase and after reaching its maximum value the Nusselt number shows large fluctuations. One can notice that the point of instability onset advances upstream as the channel's height increases.

Hence , for the same heat flux, increasing H (decreasing A) , enhances heat transfer and Nusselt number is augmented. This is an interesting result because it is different from previous studies: (Abou-Ellail and Morcos 1983), (Ozsunar, Baskaya, and Sivrioglu 2001), (Maughan and Incropera 1987) performed comparative study for different aspect ratio and

reported that Nusselt number increases with Aspect ratio (decreasing H) but for the same Grashof number.

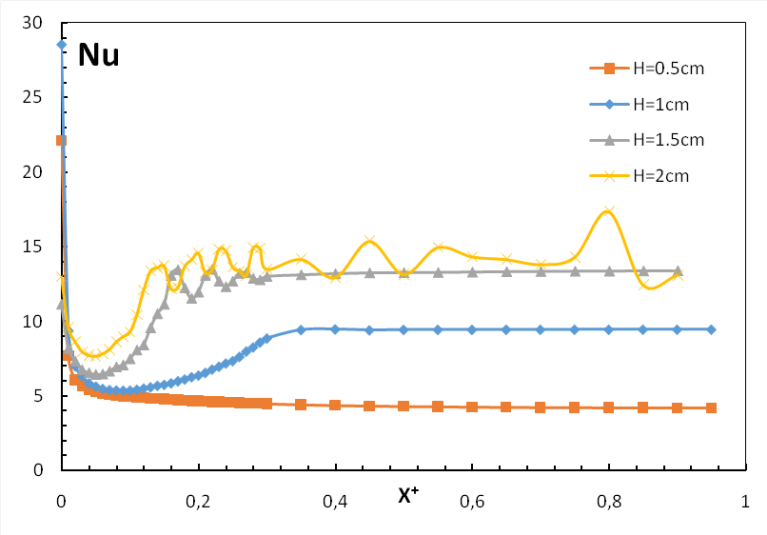

Fig. 19 Effect of channel's height on Nusselt number distribution (Re=50, Q=200 W/m^2)

To investigate the effect of channel's height for higher heat fluxes, we have tested the case of Q=600 W/m^2 at the same Reynolds number (Re=50).The flow structure and Nusselt number distribution are presented and compared to that of Q=200W/m^2 on Fig.20 and Fig.20 respectively.

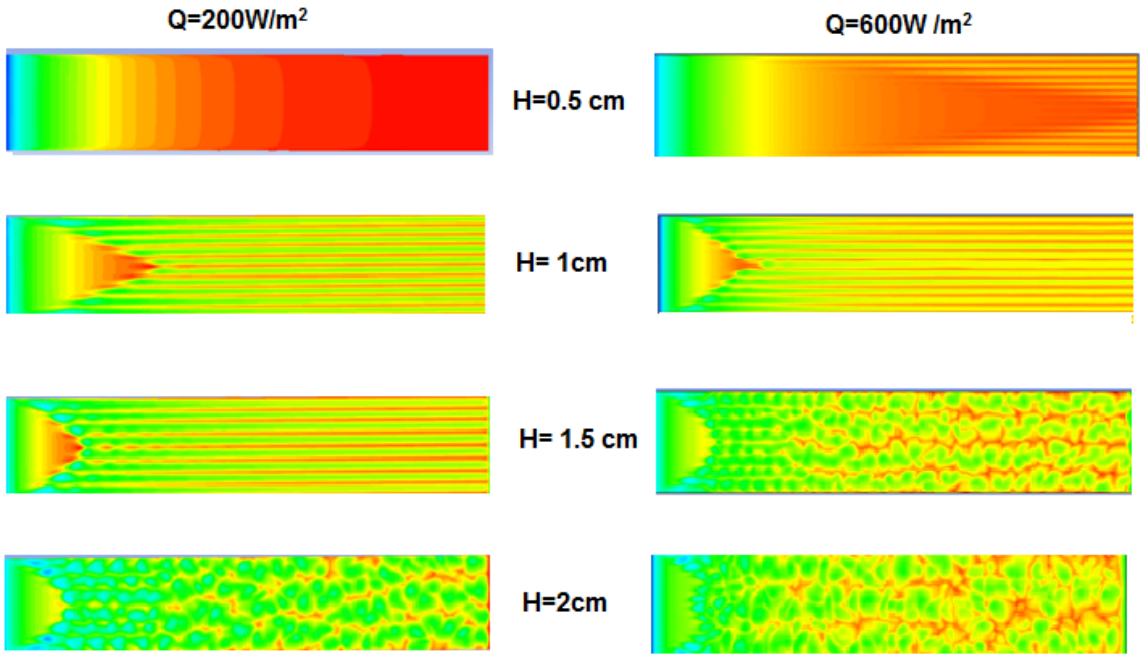

Fig. 20 Comparison of heat flux effect on longitudinal rolls development for different channel's height

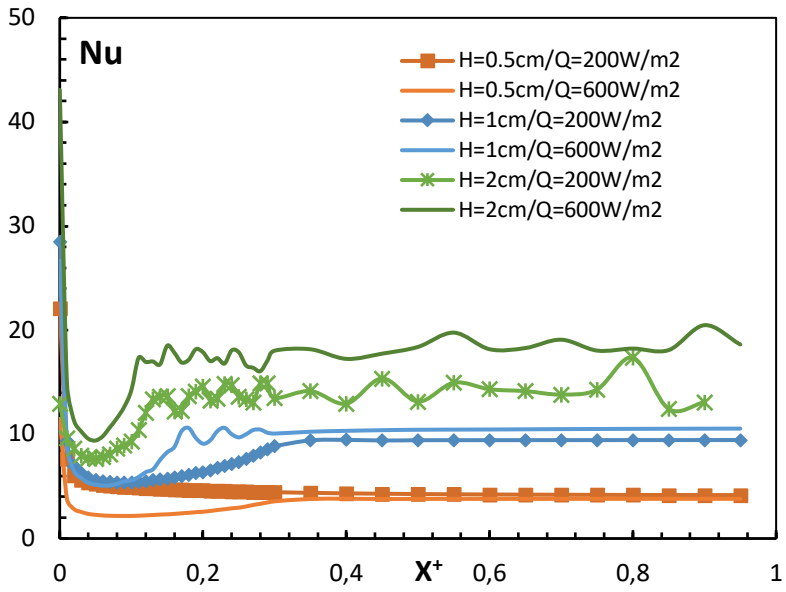

Fig.21 Spanwise averaged longitudinal distribution of Nusselt number for Q=600 W/m^2 and Q=200W/m^2, Re=50)

One can notice that for low channel's heights, increasing heat flux will enhance the onset of instability and induce the longitudinal rolls development first near the wall sides. It causes also development length Le decrease. At high channel's height, reducing surface heat flux can change the flow state from chaotic to turbulent.

From Fig.21, the main result is that for low channel's height (high aspect ratio), enhancing heat flux has not a significant effect but for higher channel's height, an augmentation of heat flux enhance buoyancy effects in the flow and causes high turbulence. This conclusion may be very useful in designing and testing solar collectors.

3-3 Effect of Reynolds number

Mixed convection flows are deeply dependent to Grashof and Reynolds numbers. In the following we will present the results obtained from investigation of Reynolds number effect on the flow structure and heat transfer enhancement in the case of channel's height of H=1cm, subjected to heat flux Q=600w/m^2. Reynolds number is varying in the range of 50 to 1000. In Fig. 21, flow pattern represented by temperature contours on the absorber (bottom plate) are shown.

For Re=50 (Ri*=13,19), the flow is characterized by three regions: the forced convection region, the instability onset region and the steady roll development region.

When Re increases, flow velocities are high, which delay the enlargement of the thermal boundary layer and inhibit the buildup of instability and (Ozsunar, Baskaya, and Sivrioglu 2001), consequently, the instability onset point is moved downstream. Moreover, the roll length development Le is increased and the roll's number decreases. This effect is more apparent for Re= 250 (Ri*=0.52), where we can observe the stretching of the forced convection region. For Re=500 to 1000 (Ri*=0.13; 0.032), inertia forces are very high, only wall sides rolls are induced and the flow reaches the exit without reaching steady state longitudinal rolls.

To investigate the effect of Re on heat transfer, we have plotted the longitudinal spanwise-averaged Nusselt number distribution versus the longitudinal position for various Reynolds number on Fig.22. The Grashof number is the same ($Gr^*=3{,}30x10^{4)}$ but Buoyancy to inertia ratio varies widely.

For small Reynolds number (Re=50, 100) corresponding to high buoyancy to inertia ratio ($Ri^*=13.19$ and 3.29 respectively), the induced secondary flow enhances heat transfer and Nusselt number is increased. As Reynolds number increases, ($Ri^*=0.52$, 0.13 and 0.032) respectively) secondary flow effects withdraw, they are almost non-existent for Re=1000 and Nusselt number variation is similar to that of forced convection. So, increasing Reynolds number, reduces fluctuations in Nusselt number and also decrease its average value. This result is in agreement with the conclusions reported by Ozsunar, Maughan and Lin.

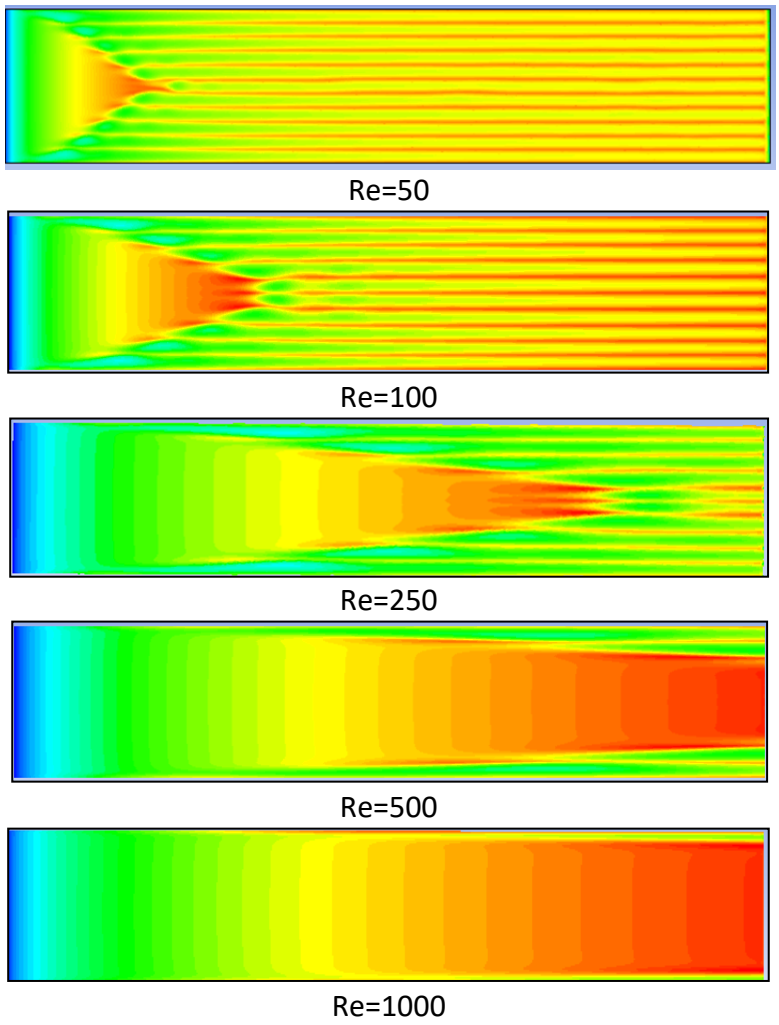

Fig.22 Contours of temperature for H=1cm, Q=600 W/m^2 and Re=50-1000

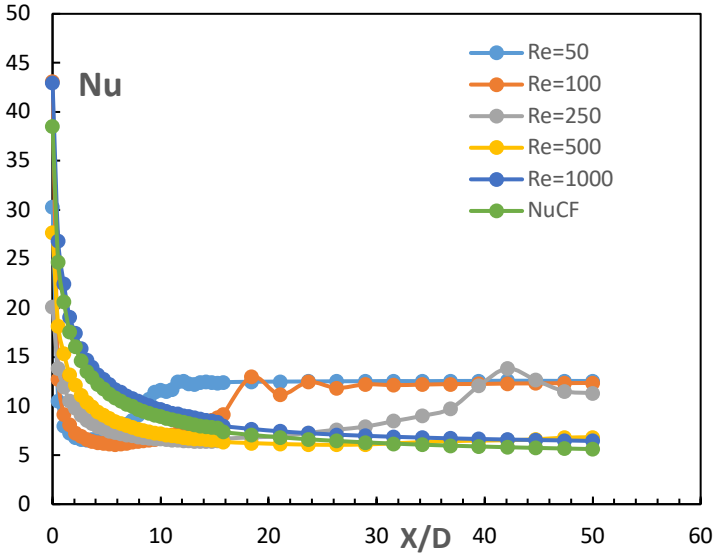

Fig. 23 Nusselt number distribution for various Reynolds number(H=1cm, Q=600 W/m^{2}Gr*=3,30x10^4)

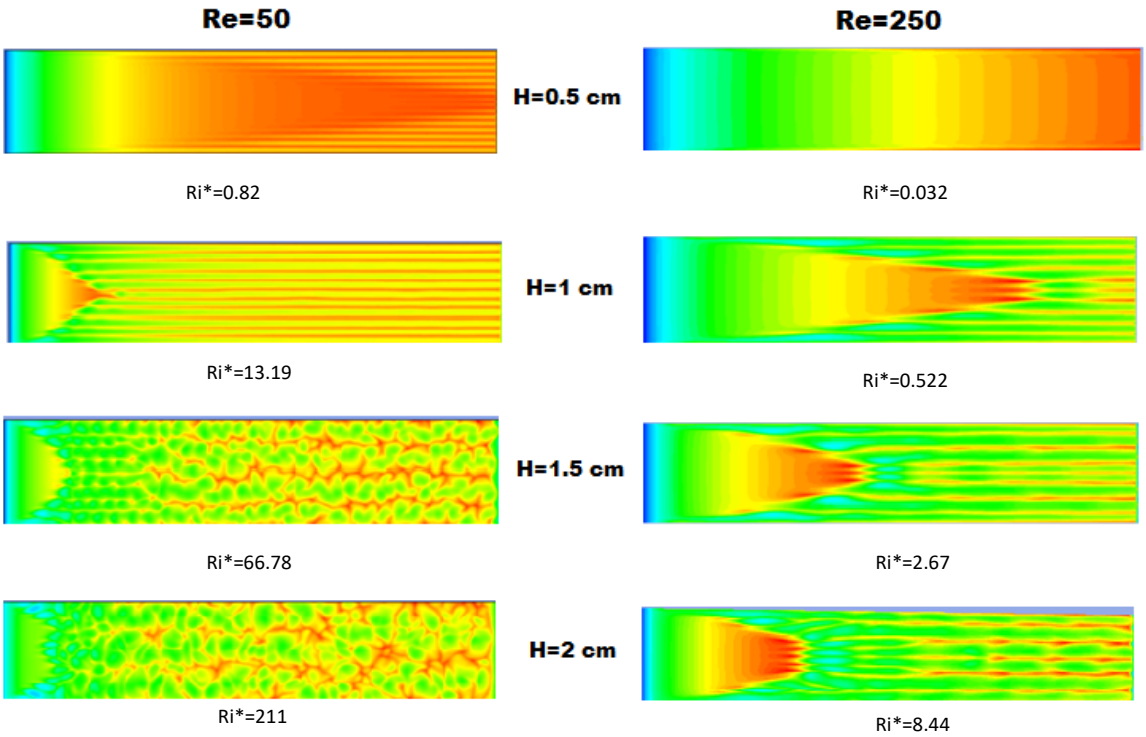

Fig. 24 Effect of Reynolds number on longitudinal rolls development for various channel's height

Fig.24 exhibits a comparison of the flow pattern of different channel's height (H=0.5cm to H=2cm) for two Reynolds number flow (Re=50 and Re=250).

At low channel's height, reducing Reynolds number promotes rolls appearance and reduces greatly the roll length development Le. At high channel's height, it causes the vortex flow to change from unsteady or chaotic to steady state with symmetric rolls splitting and merging.

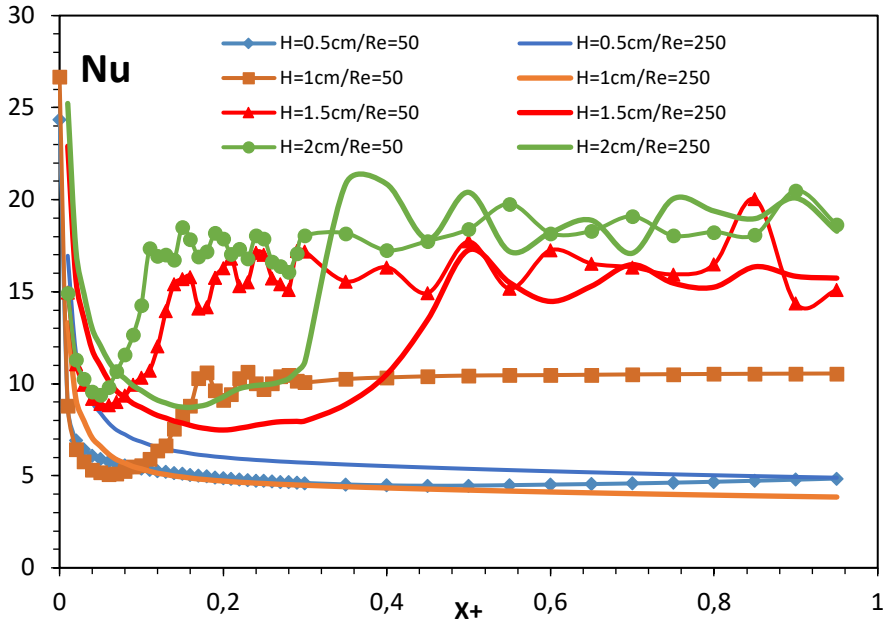

Fig.25 Spanwise-averaged longitudinal evolution of Nusselt number for various channel's height at two Reynolds number Re=50, Q=600w/m^2

Fig.25 depicts Nusselt number longitudinal evolution for various channel's heights (H=0.5-2cm) for two Reynolds numbers flow.

For low channel's height (high A), increasing Reynolds number can enhance substantially heat transfer and increased Nusselt number. For higher channel's height, increasing Re decrease Ri* from very high values to low one but still in the free convection region. One can observe that onset of secondary flow is shifted towards the exit and Nusselt number shows large fluctuations.

So, one can conclude that decreasing Reynolds number will reduce the roll development length, enlarge the mixed convection region and enhance substantially the heat transfer depending on buoyancy to inertia ratio (Ri*).

4- Conclusion

3D Numerical study of mixed convection air flow in upward solar air heater (Type I) with large spanwise aspect ratio (A = 10 to 40) was carried out. The analysis was achieved using CFD commercial code Fluent14.5 (ANSYS).

The studied domain concerns an air flow into a rectangular channel uniformly heated from below with thermally insulated lateral walls. The top wall (glazing) is subjected to external heat losses: convective heat transfer with the ambiance and radiative heat exchange with the sky. The bottom plate (absorber) is submitted to heat flux in the range of 200 to 1000 W/m^2 that represents absorbed solar radiation. The air flows at low and moderate Reynolds number from 50 to 1000.

Heat transfer characteristics of flow exhibiting longitudinal rolls was investigated in a wide range of parameters. The main objective was studying the influence of channel's height (spanwise) aspect ratio on the flow pattern and heat transfer. It was found that our results are in agreement with most of author's conclusions about PRB flows:

- Such water flows, in mixed convection air flows, longitudinal rolls are initiated by first or second mechanism depending on Ri*.

- At the same Reynolds number, increasing heat flux (modified Grashof number) will faster the onset of instability and Nusselt number is higher at the difference of forced convection flows.

- When Re increases, the instability onset point is moved downstream, the roll length development Le is increased and the roll's number decrease.

- Decreasing Reynolds number will decrease the roll development length, enlarge the mixed convection region and enhance substantially the heat transfer depending on buoyancy to inertia ratio.

Simulation results of flow visualization and Nusselt number calculation have shown that depending on Ri*, the velocity and temperature distribution in SAH vary greatly with the channel's height. The obtained results were different from previous studies. Indeed, our investigation of channel's height was achieved for the same heat flux but different Grashof number. Hence,:

- At the same heat flux and Re number increasing channel's height enhances rolls induction and decreases length roll development but beyond a certain value, the regime becomes first chaotic and then turbulent. So, reducing the channel's height can stabilize the flow. For heat transfer, Nusselt number increases with channel's height and shows large fluctuations. One can notice that the point of instability onset advances upstream as the channel's height increases.
- For low channel's height (high aspect ratio), enhancing heat flux has not a significant effect but for higher channel's height, an augmentation of heat flux enhance buoyancy effects in the flow and causes high turbulence. This conclusion may be very useful in designing and testing solar collectors. So, reducing surface heat flux can change the flow state from chaotic to turbulent.
- For low channel's height (high A), increasing Reynolds number can enhance substantially heat transfer . For higher channel's height (low A), increasing Reynolds number decrease Ri* and thus buoyancy forces. Heat transfer is reduced and so Nusselt number. So, one can conclude that reducing Reynolds number will reduce the roll development length, enlarge the mixed convection region and enhance substantially the heat transfer depending on buoyancy to inertia ratio (Ri*).

Acknowledgments: The authors thank The IUSTI (AMU, France) for providing computer resources and CFD code to achieve this study.

References

Abid, C., M. Medale, F. Papini, and P. Cerisier. 2006. 'Mixed Convection in a Horizontal Rectangular Duct Heated from Below'. *International Journal of Low-Carbon Technologies* 1 (3): 236–44. https://doi.org/10.1093/ijlct/1.3.236.

Abou-Ellail, M. M. M., and S. M. Morcos. 1983. 'Buoyancy Effects in the Entrance Region of Horizontal Rectangular Channels'. *Journal of Heat Transfer* 105 (4): 924–28. https://doi.org/10.1115/1.3245687.

Altfeld, K., W. Leiner, and M. Fiebig. 1988a. 'Second Law Optimization of Flat-Plate Solar Air Heaters. Part 2: Results of Optimization and Analysis of Sensibility to Variations of Operating Conditions'. *Solar Energy* 41 (4): 309–17. https://doi.org/10.1016/0038-092X(88)90026-6.

———. 1988b. 'Second Law Optimization of Flat-Plate Solar Air Heaters Part I: The Concept of Net Exergy Flow and the Modeling of Solar Air Heaters'. *Solar Energy* 41 (2): 127–32. https://doi.org/10.1016/0038-092X(88)90128-4.

Bammou, Lahcen, Kamal El Omari, Serge Blancher, Yves Le Guer, Brahim Benhamou, and Touria Mediouni. 2013. 'A Numerical Study of the Longitudinal Thermoconvective Rolls in a Mixed Convection Flow in a Horizontal Channel with a Free Surface'. *International Journal of Heat and Fluid Flow* 42 (August): 265–77. https://doi.org/10.1016/j.ijheatfluidflow.2013.01.017.

Benderradji, A., A. Haddad, R. Taher, M. Médale, C. Abid, and F. Papini. 2008. 'Characterization of Fluid Flow Patterns and Heat Transfer in Horizontal Channel Mixed Convection'. *Heat and Mass Transfer* 44 (12): 1465–76. https://doi.org/10.1007/s00231-008-0379-3.

Benzaoui, Abderrahmane, Xavier Nicolas, and Shihe Xin. 2005. 'Efficient Vectorized Finite-Difference Method to Solve the Incompressible Navier–Stokes Equations for 3-D Mixed-Convection Flows in High-Aspect-Ratio Channels'. *Numerical Heat Transfer, Part B: Fundamentals* 48 (3): 277–302. https://doi.org/10.1080/10407790590959825.

Boulemtafes-Boukadoum, A., and A. Benzaoui. 2014. 'CFD Based Analysis of Heat Transfer Enhancement in Solar Air Heater Provided with Transverse Rectangular Ribs'. *Energy Procedia* 50: 761–72. https://doi.org/10.1016/j.egypro.2014.06.094.

Chakkingal, Manu, Julia de Geus, Saša Kenjereš, Iman Ataei-Dadavi, M.J. Tummers, and Chris R. Kleijn. 2020. 'Assisting and Opposing Mixed Convection with Conjugate Heat Transfer in a Differentially Heated Cavity Filled with Coarse-Grained Porous Media'. *International Communications in Heat and Mass Transfer* 111 (February): 104457. https://doi.org/10.1016/j.icheatmasstransfer.2019.104457.

Elatar, Ahmed, and Kamran Siddiqui. 2014. 'The Effect of Mixed Convection on the Structure of Channel Flow at Low Reynolds Numbers'. *International Journal of Heat and Fluid Flow* 46 (April): 29–42. https://doi.org/10.1016/j.ijheatfluidflow.2013.12.005.

Everts, M., and J.P. Meyer. 2018. 'Flow Regime Maps for Smooth Horizontal Tubes at a Constant Heat Flux'. *International Journal of Heat and Mass Transfer* 117 (February): 1274–90. https://doi.org/10.1016/j.ijheatmasstransfer.2017.10.073.

Gan, Guohui. 2009. 'Effect of Air Gap on the Performance of Building-Integrated Photovoltaics'. *Energy* 34 (7): 913–21. https://doi.org/10.1016/j.energy.2009.04.003.

Gau, C., C.W. Liu, T.M. Huang, and Win Aung. 1999. 'Secondary Flow and Enhancement of Heat Transfer in Horizontal Parallel-Plate and Convergent Channels Heating from Below'. *International Journal of Heat and Mass Transfer* 42 (14): 2629–47. https://doi.org/10.1016/S0017-9310(98)00262-2.

Hegazy, Adel A. 1999. 'Optimum Channel Geometry for Solar Air Heaters of Conventional Design and Constant Flow Operation'. *Energy Conversion and Management* 40 (7): 757–774.

Hollands, K.G.T. 1979. *Free Convection in Solar Collectors*. In: Solar Energy Conversion: An Introductory Course; Course, 5th, University of Waterloo, Waterloo, Ontario, Canada, August 6-19, 1978, Selected Lectures. (A80-42435 18-44) Toronto and New York, Pergamon Press, 1979, p. 125-147.

Incropera, F. P., A. L. Knox, and J. R. Maughan. 1987. 'Mixed-Convection Flow and Heat Transfer in the Entry Region of a Horizontal Rectangular Duct'. *Journal of Heat Transfer* 109 (2): 434. https://doi.org/10.1115/1.3248100.

Kalogirou, Soteris A. 2004. 'Solar Thermal Collectors and Applications'. *Progress in Energy and Combustion Science* 30 (3): 231–95. https://doi.org/10.1016/j.pecs.2004.02.001.

Kamotani, Y., S. Ostrach, and H. Miao. 1979. 'Convective Heat Transfer Augmentation in Thermal Entrance Regions by Means of Thermal Instability'. *Journal of Heat Transfer* 101 (2): 222. https://doi.org/10.1115/1.3450950.

Lin, W. L., and T. F. Lin. 1996a. 'Unstable Aiding and Opposing Mixed Convection of Air in a Bottom-Heated Rectangular Duct Slightly Inclined From the Horizontal'. *Journal of Heat Transfer* 118 (1): 47. https://doi.org/10.1115/1.2824066.

Lin, W.L., and T.F. Lin. 1996b. 'Experimental Study of Unstable Mixed Convection of Air in a Bottom Heated Horizontal Rectangular Duct'. *International Journal of Heat and Mass Transfer* 39 (8): 1649–63. https://doi.org/10.1016/0017-9310(95)00256-1.

Maughan, J.R., and F.P. Incropera. 1987. 'Experiments on Mixed Convection Heat Transfer for Airflow in a Horizontal and Inclined Channel'. *International Journal of Heat and Mass Transfer* 30 (7): 1307–18. https://doi.org/10.1016/0017-9310(87)90163-3.

———. 1990. ‘Regions of Heat Transfer Enhancement for Laminar Mixed Convection in a Parallel Plate Channel’. *International Journal of Heat and Mass Transfer* 33 (3): 555–70. https://doi.org/10.1016/0017-9310(90)90189-2.

Meyer, J.P., and M. Everts. 2018. ‘Single-Phase Mixed Convection of Developing and Fully Developed Flow in Smooth Horizontal Circular Tubes in the Laminar and Transitional Flow Regimes’. *International Journal of Heat and Mass Transfer* 117 (February): 1251–73. https://doi.org/10.1016/j.ijheatmasstransfer.2017.10.070.

Meyer, J.P., M. Everts, N. Coetzee, K. Grote, and M. Steyn. 2019. ‘Heat Transfer Coefficients of Laminar, Transitional, Quasi-Turbulent and Turbulent Flow in Circular Tubes’. *International Communications in Heat and Mass Transfer* 105 (June): 84–106. https://doi.org/10.1016/j.icheatmasstransfer.2019.03.016.

Moffat, H. K. 1988. ‘Three-Dimensional Flow Effects in Silicon CVD in Horizontal Reactors’. *Journal of The Electrochemical Society* 135 (2): 459. https://doi.org/10.1149/1.2095638.

Moffat, Harry, and Klavs F. Jensen. 1986. ‘Complex Flow Phenomena in MOCVD Reactors’. *Journal of Crystal Growth* 77 (1–3): 108–19. https://doi.org/10.1016/0022-0248(86)90290-3.

Nicolas, Xavier. 2002. ‘Revue bibliographique sur les écoulements de Poiseuille–Rayleigh–Bénard : écoulements de convection mixte en conduites rectangulaires horizontales chauffées par le bas’. *International Journal of Thermal Sciences* 41 (10): 961–1016. https://doi.org/10.1016/S1290-0729(02)01374-1.

Ostrach, S., and Y. Kamotani. 1975. ‘Heat Transfer Augmentation in Laminar Fully Developed Channel Flow by Means of Heating From Below’. *Journal of Heat Transfer* 97 (2): 220. https://doi.org/10.1115/1.3450344.

Ozsunar, A., S. Baskaya, and M. Sivrioglu. 2001. ‘Numerical Analysis of Grashof Number, Reynolds Number and Inclination Effects on Mixed Convection Heat Transfer in Rectangular Channels’. *International Communications in Heat and Mass Transfer* 28 (7): 985–94. https://doi.org/10.1016/S0735-1933(01)00302-5.

Rahli, O., R. Bennacer, K. Bouhadef, and D. E. Ameziani. 2011. ‘Three-Dimensional Mixed Convection Heat and Mass Transfer in a Rectangular Duct: Case of Longitudinal Rolls’. *Numerical Heat Transfer, Part A: Applications* 59 (5): 349–71. https://doi.org/10.1080/10407782.2011.549081.

R.K. Shah and A.L. London. 1978. *Laminar Flow Forced Convection in Ducts*. Elsevier. https://doi.org/10.1016/C2013-0-06152-X.

Sun, Wei, Jie Ji, and Wei He. 2010. ‘Influence of Channel Depth on the Performance of Solar Air Heaters’. *Energy* 35 (10): 4201–7. https://doi.org/10.1016/j.energy.2010.07.006.

Taher, R., and C. Abid. 2018. ‘Experimental Determination of Heat Transfer in a Poiseuille-Rayleigh-Bénard Flow’. *Heat and Mass Transfer* 54 (5): 1453–66. https://doi.org/10.1007/s00231-017-2220-3.

Uchida. 1966. ‘Forced Convective Heat Transfer between Horizontal Flat Plates’. *International Journal of Heat and Mass Transfer* 9 (8): 803–17. https://doi.org/10.1016/0017-9310(66)90007-X.

Wessels, Malte, Daniel Schmeling, Johannes Bosbach, and Claus Wagner. 2019. ‘On the Impact of the Aspect Ratio on the Formation of Large-Scale Structures in Turbulent Mixed Convection in a Cuboidal Sample’. *International Journal of Heat and Fluid Flow* 76 (April): 231–41. https://doi.org/10.1016/j.ijheatfluidflow.2019.01.004.

Yadav, Anil Singh, and J.L. Bhagoria. 2013. ‘Heat Transfer and Fluid Flow Analysis of Solar Air Heater: A Review of CFD Approach’. *Renewable and Sustainable Energy Reviews* 23 (July): 60–79. https://doi.org/10.1016/j.rser.2013.02.035.

Zhu, Rongjia, Ping Zhou, Jialing Li, and Chenn Q. Zhou. 2020. ‘CFD Model Evaluation in Mixed Convection with High Richardson Number’. *International Journal of Heat and Mass Transfer* 149 (March): 119133. https://doi.org/10.1016/j.ijheatmasstransfer.2019.119133.